



Determination of the critical aragonite saturation state under which  
skeleton structures of the cold-water coral  
*Lophelia pertusa* begin to dissolve

## Diplomarbeit

vorgelegt von

**Janett Voigt**

aus Bautzen  
geboren am  
04.06.1985

angefertigt an der  
Universität Rostock  
Institut für Biowissenschaften  
Abteilung Meeresbiologie

im Oktober 2010

Cover picture

Drawing of *Lophelia pertusa* (as *Madrepora pertusa*) by Johann Ernst Gunnerus (1768).

Taken from Moen 2006

1. Gutachter: PD Dr. Stefan Forster, Universität Rostock

Institut für Biowissenschaften

Abteilung Meeresbiologie

2. Gutachter: Prof. Dr. Ulf Riebesell, IFM-GEOMAR

Leibniz-Institut für Meereswissenschaften an der Universität Kiel

Marine Biogeochemie

Biologische Ozeanographie

Düsternbrooker Weg 20

24105 Kiel

# Index

<b>Index</b>	<b>3</b>
<b>List of figures</b>	<b>5</b>
<b>List of tables</b>	<b>7</b>
<b>List of abbreviations</b>	<b>8</b>
<b>Abstract</b>	<b>9</b>
<b>Kurzfassung</b>	<b>10</b>
<b>1. Introduction</b>	<b>11</b>
1.1 Systematic classification and biological categorisation	11
1.2 Distribution	11
1.3 Environmental controls	12
1.4 Biology	13
1.4.1 Anatomy	13
1.4.2 Morphology	13
1.4.3 Growth	13
1.4.4 Biomineralization	14
1.4.5 Nutrition	15
1.4.6 Reproduction	15
1.5 Ecosystem cold-water coral reef	16
1.5.1 Comparison between tropical, shallow and cold-water reefs	16
1.5.2 Micro- and macrohabitats	18
1.5.3 Bioerosion	19
1.6 Threats to reef structures	20
1.7 Climate change and ocean acidification	20
1.8 Skeletal characterisation	27
1.8.1 Structure	27
1.8.2 Composition	27
1.8.3 Comparison between biogenic and abiogenic aragonite	28
1.9 Dissolution kinetics	29
1.10 Thesis outline	30
<b>2. Materials and Methods</b>	<b>32</b>
2.1 Main experiment	32
2.2 Media preparation	34
2.2.1 Water filtration	34
2.2.2 Acidification	34
2.2.3 Coral material	34
2.3 Preliminary tests	36
2.3.1 Test run I: Dissolution experiment with coral rubble	36
2.3.2 Test run II: Sealing experiments	36
2.3.3 Test run III: Elimination of possible micro-organisms	37
2.3.4 Test run IV: Eliminating organic remains	37
2.4 Control experiment	38

2.5 Determination of organic content in coral skeleton	39
2.6 Measurements	40
2.6.1 Measuring total alkalinity	40
2.6.2 pH measurement	41
2.6.3 Measuring dissolved inorganic carbon	41
2.7 Determination of aragonite saturation state	42
2.8 Examination of skeleton surface structure	42
2.9 Data processing	42
<b>3. Results</b>	<b>44</b>
3.1 Preliminary tests	44
3.2 Main experiment	45
3.3 Control experiment	49
3.4 Determination of organic content in skeleton	52
3.5 Examination of skeleton surface structure	53
<b>4. Discussion</b>	<b>60</b>
4.1 Precision of measured data	60
4.2 Main experiment	60
4.3 Control experiment	63
4.4 Summary of main and control experiment	64
4.5 Determination of organic content in coral skeleton	65
4.6 Comparison between coral and abiogenic aragonite density	66
4.7 Examination of skeleton surface structure	67
4.8 Dissolution kinetics	68
4.9 Conclusion	68
<b>5. Significance of work</b>	<b>70</b>
<b>6. Outlook</b>	<b>71</b>
<b>Acknowledgement</b>	<b>73</b>
<b>References</b>	<b>74</b>
<b>Appendix</b>	<b>81</b>
<b>Declaration of Academic Integrity / Selbstständigkeitserklärung</b>	<b>91</b>

## List of figures

Figure 1.1 Distribution chart of <i>Lophelia pertusa</i>	11
Figure 1.2 Schematic picture of the different macrohabitats of a <i>Lophelia pertusa</i> reef	18
Figure 1.3 Graph showing relative changes in inorganic carbon species in response to changes in atmospheric CO <sub>2</sub> concentrations	21
Figure 1.4 Distribution of aragonite saturation horizon in the global oceans	23
Figure 1.5 Maps illustrating the decline in $\Omega_{Ar}$ in the global oceans	25
Figure 1.6 SEM images showing aragonite crystals accreted by corals, reared in seawater with given ranges of $\Omega_{Ar}$	27
Figure 2.1 Diagram presenting the experimental set-up	33
Figure 2.2 Map of the locations of sampled coral reefs	35
Figure 2.3 Set-up for sub-experiment two	39
Figure 3.1 Graphs a-c illustrating dissolution of the skeleton fragments with time by rising $\Omega_{Ar}$ for all three treatments	46
Figure 3.2 Graphs a-c show increasing $\Omega_{Ar}$ with time due to dissolution of coral skeleton fragments for the different treatments	47
Figure 3.3 Graph presents the development of $\Omega_{Ar}$ for all three pCO <sub>2</sub> treatments due to dissolution of the fragments	48
Figure 3.4 Graph illustrating an increase in $\Omega_{Ar}$ resulting from dissolution of coral skeletons for the control treatment	48
Figure 3.5 Development of $\Omega_{Ar}$ for the blanks of the different treatments due to outgassing via sampling	49
Figure 3.6 Graphs a, b showing the development of $\Omega_{Ar}$ due to dissolution of coral fragments for the different experimental set-ups	50
Figure 3.7 Graphs a, b showing increase in $\Omega_{Ar}$ for S <sub>I</sub> (a) and S <sub>II</sub> (b) caused by dissolving of coral material	51
Figure 3.8 Graph for control experiment illustrating dissolution of coral skeletons by increasing $\Omega_{Ar}$ with time for the different set-ups	51
Figure 3.9 Blanks for the control experiment presenting the development of $\Omega_{Ar}$	52
Figure 3.10 SEM images of fragment samples of the control	54
Figure 3.11 SEM images of coral fragments from the 1200 ppm CO <sub>2</sub> treatment	55
Figure 3.12 SEM images of coral samples of the 1800 ppm CO <sub>2</sub> treatment	56
Figure 3.13 SEM images of coral fragments from the 2500 ppm pCO <sub>2</sub> treatment	57

Figure 3.14 SEM images of coral fragment from the 2500 ppm CO <sub>2</sub> treatment exhibiting mechanical damage and dissolution spots on septa	58
Figure 3.15 SEM images showing crystal morphology	59
Figure 4.1 Graph showing increase in $\Omega_{Ar}$ with time due to dissolution of coral fragments from the main and control experiment revealing a critical $\Omega_{Ar} < 1$	65

## List of tables

Table 1.1 Comparison between shallow and deep-water reefs	17
Table 3.1 Ash-free dry weight and percentage weight loss of white and red types of <i>L. pertusa</i>	53
Table 4.1 Mean standard deviation and coefficient of variance for both experiments	60

## List of abbreviations

$\Omega_{Ar}$	aragonite saturation state
AFDM	ash-free dry mass
ASH	aragonite saturation horizon
DIC	dissolved inorganic carbon
DOC	dissolved organic carbon
e.m.f.	electromotive force
IPCC	Intergovernmental Panel on Climate Change
MET	monotonic equivalent-point titration
NSW	natural seawater
pCO <sub>2</sub>	partial pressure of CO <sub>2</sub>
PTFE	polytetrafluorethylene, common name: teflon
S <sub>I</sub>	sub-experiment one of the control experiment
S <sub>II</sub>	sub-experiment two of the control experiment
SEM	scanning electron microscopy
TA	total alkalinity



## Abstract

The scleractinian *Lophelia pertusa* is a cosmopolitan reef-forming cold-water coral and creates a habitat for a diverse associated community. This ecosystem, however, is threatened by ocean acidification due to declining pH and shoaling of the carbonate saturation horizon resulting in dissolution of coral skeletons. The aragonite saturation state ( $\Omega_{Ar}$ ) given in literature refers to the pure mineral but organic compounds within the skeleton might have an impact on dissolution behaviour and thus could influence the solubility product of aragonite. In this study the critical  $\Omega_{Ar}$ , under which aragonite starts to dissolve, was determined for dead skeleton framework of *L. pertusa* through manipulating natural seawater by acidification (by use of HCl and Na<sub>2</sub>CO<sub>3</sub>) and bubbling with CO<sub>2</sub>-enriched air. Moreover, the organic portion of the skeleton was quantified by determining the ash-free dry weight. Additionally, scanning electron microscopy images were taken after the dissolution experiment to examine visible dissolution effects on the skeleton surface. Measurements revealed an  $\Omega_{Ar}$  range of 0.795-0.971. Combustion of skeleton fragments of the white and red colour variety of *L. pertusa* presented an organic content of 3.37 and 3.11 % of total weight, respectively. This relatively high organic fraction within the skeleton could explain the low saturation state obtained which is below the generally stated threshold of  $\Omega_{Ar} = 1$ . Since the dead framework constitutes the major part of a cold-water reef the obtained saturation state might be regarded as the critical  $\Omega_{Ar}$  for an entire *L. pertusa* reef. Consequently, this low critical saturation state could indicate that *Lophelia pertusa* reefs are probably more resistant to ocean acidification than thought before resulting in significant implications for future predicting models.

## Kurzfassung

Die weltweit verbreitete Kaltwasserkoralle *Lophelia pertusa* bietet mit ihrer verzweigten Skelettstruktur Lebensraum für eine artenreiche Fauna. Die zunehmende Versauerung der Meere führt jedoch zu einem Absinken des pH-Wertes und damit verbunden zu einem Anstieg des Aragonitsättigungshorizontes. Unterhalb dieses Schwellenwertes sind die aus Aragonit aufgebauten Korallenskelette vom Auflösen bedroht und somit ist das gesamte Ökosystem der Korallenriffe gefährdet. Der Grad der Aragonitsättigung ( $\Omega_{Ar}$ ) wird in der Literatur stets für das chemisch reine Mineral angegeben, obwohl zahlreiche Studien belegen, dass Korallenskelette nicht nur aus Kalziumkarbonat bestehen, sondern auch organische Bestandteile aufweisen. Diese könnten Einfluss auf das Lösungsverhalten der Karbonate und damit auf den Sättigungsgrad haben. Das Ziel dieser Arbeit war es, den kritischen Grad der Aragonitsättigung, dessen Unterschreitung ein Auflösen von Aragonit bedeutet, anhand von totem Skelettmaterial zu bestimmen. Dies erfolgte durch Ansäuerung von natürlichem Seewasser mittels verschiedener Methoden (Zugabe von HCl und Na<sub>2</sub>CO<sub>3</sub>, Manipulation mit CO<sub>2</sub> angereicherter Luft). Der Anteil der organischen Substanz innerhalb der Skelette wurde über das aschefreie Trockengewicht ermittelt. Elektronenmikroskopische Untersuchungen von Korallenfragmenten zeigten sichtbare Auflösung der Oberflächenstrukturen. Die angewandten Methoden der CO<sub>2</sub>-Manipulation ergaben einen kritischen Sättigungsgrad von 0,795-0,971. Der Anteil organischer Bestandteile der Skelette betrug durchschnittlich 3,37 und 3,11 % der Gesamtmasse für die weiße bzw. rote Farbvariante von *L. pertusa*. Dieser relativ hohe organische Anteil innerhalb der Skelette könnte den hier ermittelten Sättigungsgrad, welcher deutlich unterhalb des Grenzwertes von  $\Omega_{Ar} = 1$  liegt, erklären. Da totes Skelettmaterial den größten Teil eines Kaltwasserriffes ausmacht, kann der ermittelte Sättigungsgrad als kritischer Grenzwert eines gesamten *L. pertusa* Riffes betrachtet werden. Der niedrige Grad der Aragonitsättigung sollte in zukünftigen Anwendung von Klimaszenarien auf Kaltwasserkorallen berücksichtigt werden, da er darauf hinweist, dass *Lophelia pertusa* noch nicht in dem Maß von der Ozeanversauerung betroffen ist, als bisher vermutet.

## 1. Introduction

### 1.1 Systematic classification and biological categorisation

*Lophelia pertusa* was first described by Linnaeus in 1758. It belongs to the phylum Cnidaria, class Anthozoa, subclass Hexacorallia, order Scleractinia, family Caryophylliidae.

*L. pertusa* is classified as an azooxanthellate, habitat-forming organism. Azooxanthellate corals do not host symbiotic microalgae in their endodermal cells, deeper forms due to lack of light for photosynthesis.

### 1.2 Distribution

*Lophelia pertusa* is a cosmopolitan coral growing in dark, cold waters and was recorded from the Atlantic Ocean (North and Northeast Atlantic, Gulf of Mexico, Caribbean Sea), parts of the Mediterranean Sea, parts of Northeast Pacific and Indian Ocean (Figure 1.1) (Freiwald *et al.* 2004, Roberts *et al.* 2009, Rogers 1999).

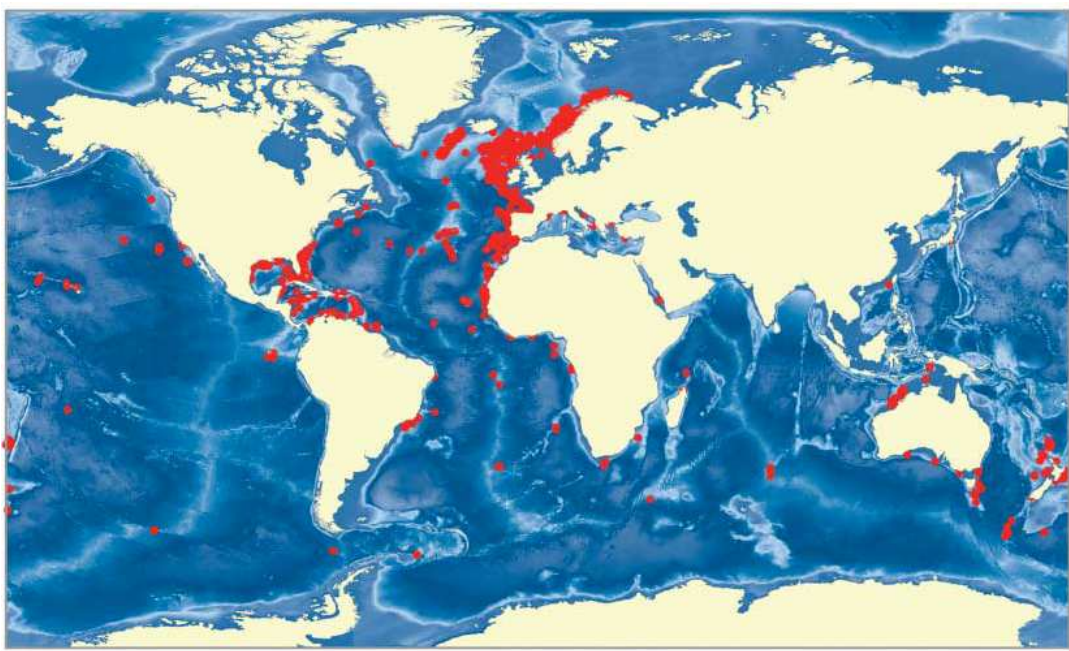


**Figure 1.1** Distribution chart of *Lophelia pertusa*. From Roberts *et al.* (2006)

*L. pertusa* can be found on continental margins and slopes, banks, carbonate mounds, submarine plateaus, seamounts, canyons, and mid-oceanic ridges but also in fjords at

higher latitudes (Freiwald *et al.* 2004, Roberts *et al.* 2006, Roberts *et al.* 2009, Rogers 1999, Wheeler *et al.* 2007).

*L. pertusa* occurs at depths ranging from less than 50 m in fjords in higher latitudes to 3600 m at the Mid-Atlantic Ridge in the tropics (Freiwald *et al.* 2004, Roberts *et al.* 2006, Rogers 1999) but it is commonly found in 200-1000 m water depth (Rogers 1999, Rogers 2004). Depth occurrence depends on properties of the water mass (Rogers 1999).

### 1.3 Environmental controls

*Lophelia pertusa* requires strong currents and hard substrate but also certain water mass characteristics for settlement and survival (see also Table 1.1).

Depending on their distribution the corals need upwelled water, when found on shallow fjords, or strong currents for sufficient supply of food and oxygen (Davies *et al.* 2008, Roberts *et al.* 2009).

This coral occurs at salinities ranging from 35-37 (Davies *et al.* 2008, Dullo *et al.* 2008, Freiwald *et al.* 2004, Rogers 1999) but the salinity at the Norwegian sites differs because of outflow from the Baltic Sea and high river discharge which shows considerable high salinity tolerance of *L. pertusa* (Dullo *et al.* 2008).

Rocks, ice-rafted debris, slopes of submarine canyons or carbonate precipitations (mounds, authigenic carbonates); even man-made structures are used for larval settling (Roberts *et al.* 2006, Rogers 1999).

*L. pertusa* tolerates different temperatures depending where it lives but occurrence seems to be limited to the range of 4-12°C at North Atlantic sites (Rogers 1999).

This cold-water coral has a low oxygen consumption which indicates low metabolic rates, typical for organisms in deeper waters due to low temperatures (Dodds *et al.* 2007). However, it was shown that oxygen concentrations may be an important factor for occurrences of *L. pertusa* (Davies *et al.* 2008).

Results from sedimentation experiments suggest that *L. pertusa* can tolerate a relatively severe sediment load and even complete burial for short periods (24-48 hours) (CSA International, Inc. 2007). High sedimentation, however, could clog the feeding apparatus resulting in anoxia which in turn would lead to reduced growth rates (Rogers 1999).

## 1.4 Biology

### 1.4.1 Anatomy

Cnidarians are classified by having biradial symmetry as well as tentacles with cnidocytes which are specialized cells used for protection and capture of prey. The body consists of a sac-like gastrovascular cavity with a mouth surrounded by tentacles and mesenteries inside the cavity.

The order Scleractinia or stony corals is characterized by a calcareous exoskeleton and paired, complete mesenteries. Number of tentacles and septa are in multiples of six. The skeleton of an individual polyp is known as a corallite. It is secreted by the aboral epidermal cells which initially form a basal plate and a cup enclosing the lower part of the polyp's stalk and is then called theca. The interior of the cup contains radially-aligned septa which are projecting upwards from the base and are secreted by the mesenteries.

### 1.4.2 Morphology

Different colour varieties of *L. pertusa* were found to be intraspecific variations (Rogers 1999). The most common colour variety is the white one but there are also yellow, orange, and red variations (Freiwald *et al.* 2004, Roberts *et al.* 2009, Rogers 1999). In the Northeast Atlantic white and red types dominate (Rogers 1999).

Distinct morphotypes of *L. pertusa* were also reported (Freiwald *et al.* 1997a) which show different skeletal anatomies and corallite densities in response to environmental conditions (CSA International, Inc. 2007).

### 1.4.3 Growth

Since *Lophelia pertusa* thrives in cold waters, it is a long-lived and relatively slow growing coral (Rogers 1999). Different growth rates were reported depending on the method used. In general, growth rates of *L. pertusa* range from 4-25 mm/ year (CSA International, Inc. 2007, Dodds 2007, Freiwald *et al.* 2004, Roberts *et al.* 2009).

Coral growth is expressed as longitudinal extension and thickening, the latter result in growth bands, whereas extension rates are much higher (5 mm/ year) than thickening (100  $\mu$ m/ year) (Cohen *et al.* 2006, Roberts *et al.* 2009).

Growth of polyps as well as that of whole reef framework depend on temperature and the aragonite saturation horizon (see chapter 1.7 Climate change and ocean acidification)

(for example Cohen *et al.* 2006, Roberts *et al.* 2009, Turley *et al.* 2007). Furthermore, growth is controlled by food supply and reproduction cycles (CSA International, Inc. 2007, Freiwald *et al.* 2004, Roberts *et al.* 2009).

Given the low growth rates and their longevity, reefs of some tens of metres in thickness must have an age of at least thousands of years and living coral structures found at the Sula Reef are more than 8000 years old (Freiwald *et al.* 2004, Rogers 2004).

#### 1.4.4 Biomineralization

The mechanism of biomineralization or calcification is still unclear; however, there are different theories (for example Allemand *et al.* 2004, Cuif and Dauphin 2005b, Kleypas and Yates 2009, Marubini *et al.* 2008, Meibom *et al.* 2007). This mechanism was exclusively studied on tropical corals but it should proof to be similar for all stony corals.

Biomineralization can be described by following equation:



In laboratory experiments calcification was determined by means of buoyant weight changes,  $^{45}\text{Ca}$  uptake, densitometry, tomography, changes in alkalinity, and extension rates (Freiwald *et al.* 2004, Kleypas and Langdon 2006). Coral calcification is influenced by environmental conditions like pH, temperature,  $\text{CO}_3^{2-}$  ion concentration, aragonite saturation state ( $\Omega_{\text{Ar}}$ ), and nutrient supply (Kleypas *et al.* 2006, Kleypas and Langdon 2006).

Biomineralization is mediated through the calcicoblastic epithelium in the aboral ectoderm, and the calcification site is separated from seawater (Allemand *et al.* 2004, Cohen and Holcomb 2009b). A few studies point out that corals use both,  $\text{CO}_2$  from metabolism and  $\text{HCO}_3^-$  from seawater (Allemand *et al.* 2004, Furla *et al.* 2000). At the calcification site  $\text{HCO}_3^-$  has to be converted into  $\text{CO}_3^{2-}$  and is transported by special carriers (Allemand *et al.* 2004). High levels of carbonate species are found at calcification centres indicating a carbon concentrating mechanism (Allemand *et al.* 2004, Cohen and Holcomb 2009b, Furla *et al.* 2000).

The calcium needed for biomineralization is taken up from the surrounding seawater. The  $\text{Ca}^{2+}$  is transported by special carriers (Allemand *et al.* 2004). This transport requires much

energy which is provided by the numerous mitochondria at the calcification site (Allemand *et al.* 2004).

Corals can elevate their internal pH at calcification sites which favours the conversion of  $\text{HCO}_3^-$  into  $\text{CO}_3^{2-}$  (Blamart *et al.* 2007, Cohen and Holcomb 2009b, Marubini *et al.* 2008, Ries *et al.* 2009). This pH elevation results in a rise of internal  $\text{CO}_3^{2-}$  ion concentration above that of seawater (Cohen *et al.* 2009a, Cohen and Holcomb 2009b). Nevertheless, corals are very sensitive to small changes in carbonate concentrations of seawater (Cohen *et al.* 2009a).

#### 1.4.5 Nutrition

Since cold-water corals live in the dark and host no symbionts they depend on heterotrophic feeding (CSA International, Inc. 2007). It is most likely that *Lophelia pertusa* is an opportunistic consumer able to feed on dissolved and particulate organic matter, bacteria, faecal pellets, both phyto- and zooplankton, detritus, suspended sediments, and resuspended material (Dodds 2007, Roberts *et al.* 2006, Roberts *et al.* 2009). *L. pertusa* occurs in nutrient-rich environments because of strong currents at coral sites supplying the mentioned food sources (Roberts *et al.* 2006, Roberts *et al.* 2009).

#### 1.4.6 Reproduction

Only little is known about the reproduction of *L. pertusa*. Asexual reproduction, for example fragmentation and breakage, is important for establishing new colonies within the reef area (CSA International, Inc. 2007).

*L. pertusa* has separate sexes and dispersive planktonic larvae are very likely (CSA International, Inc. 2007, Roberts *et al.* 2006, Rogers 1999). Spawning times of *L. pertusa* are different at distinct locations probably due to different environmental parameters like temperature and food supply (CSA International, Inc. 2007).

Investigation of larval biology and dispersal is still in its infancy because direct observation is difficult.

### 1.5 Ecosystem cold-water coral reef

*Lophelia pertusa* can be regarded as a bioengineer because it can alter its environment and provides a three-dimensional framework which in turn hosts a diverse community (Freiwald *et al.* 2004, Roberts *et al.* 2006, Roberts *et al.* 2009, Rogers 1999). Given their longevity cold-water reefs might be speciation centres comparable to seamounts and are believed to have been refugia during glacial periods (Roberts *et al.* 2006).

The whole framework creating the ecosystem has distinct functions like reduction of current speed thus more food particles are available (see also Table 1.1) (de Haas *et al.* 2009, Freiwald *et al.* 2004, Rogers 2004). Another function is the stabilization of sediment (Roberts *et al.* 2009, Wheeler *et al.* 2007).

#### 1.5.1 Comparison between tropical, shallow and cold-water reefs

Both ecosystems are polyphyletic assemblages of cnidarians with very different coral species. Table 1.1 summarizes similarities and differences between both ecosystems.



**Table 1.1** Comparison between shallow and deep-water reefs.Modified from Freiwald *et al.* (2004)

	<b>Cold-water coral reef</b>	<b>Warm-water coral reef</b>
Distribution	Global – potentially in all seas, at all latitudes	Global – in subtropical and tropical seas between 30° N and 30° S
Coverage	Unknown – indication that global coverage could equal, or even exceed, that of warm-water reefs Highest coverage – unknown but 2000 km <sup>2</sup> in Norwegian waters	284,300 km <sup>2</sup>  Highest coverage – 51,020 km <sup>2</sup> in Indonesia
Largest reef complex	Unknown – Røst Reef in Norway to date considered as the largest (100 km <sup>2</sup> )	Great Barrier Reef in Australia (> 30,000 km <sup>2</sup> )
Substratum	Any available hard substrate	Any available hard substrate
Temperature range	4 – 14°C	20 – 29°C (at least 18°C throughout the year)
Salinity range	32 – 38.8 but mostly 35 – 37	33 – 36
Depth range	39 – 3600 m but mainly at 200 – 1000 m	0 – 100 m
Nutrition	Most likely phyto- and zooplankton, suspended organic matter, detritus, bacteria	Photosynthesis and suspended organic matter
Symbiotic algae	No	Yes
Nutrients	High nutrients supplied by currents, surface production	Low nutrients – supply by symbiotic algae
Growth rate	4 – 25 mm/ year	Up to 150 mm/ year
Spawning	Most likely not synchronous	Mostly broadcast spawning
Number of reef-building coral species	Few – only 6 primary species	About 800
Reef composition	Mostly composed of one or only few species	Mostly composed of numerous species
Age of living reefs	Up to 8000 years	6000 – 9000 years
Endemism	Unknown – to date no endemic species found	Several endemic species
Ecological importance	Reefs provide habitat, feeding grounds, recruitment and nursery functions for many deep-water species, including commercial fish, number of associated species and their ecological importance/ value still unknown	Reefs provide habitat, feeding grounds, recruitment and nursery functions; estimations of 1 million species associated, approximately 4000 coral fish species
Socio-economic importance	Unknown – importance indicated for local fisheries, including coastal line/ net fisheries and deep-water fisheries	Reefs provide coastal protection, source of livelihood for > 1 billion people, net potential benefits estimated at US \$ 30 billion/ year

### 1.5.2 Micro- and macrohabitats

Microhabitats can be found on living corals but also on dead corals and detritus (Roberts *et al.* 2009, Rogers 1999). Eroding organisms create cavities inside the coral skeleton (Beuck and Freiwald 2005, Roberts *et al.* 2009, Rogers 1999) and the free space between branches provides habitats for small epibenthic and associated fauna (Roberts *et al.* 2009, Rogers 1999).

The provided macrohabitats show a high biodiversity because the corals create a lot of niches for organisms (Freiwald *et al.* 2004, Roberts *et al.* 2009, Rogers 1999). Three typical macrohabitats are commonly distinguished: the zone of living corals, dead framework and the coral rubble zone (Figure 1.2) (Freiwald *et al.* 2004, Roberts *et al.* 2009, Rogers 1999).

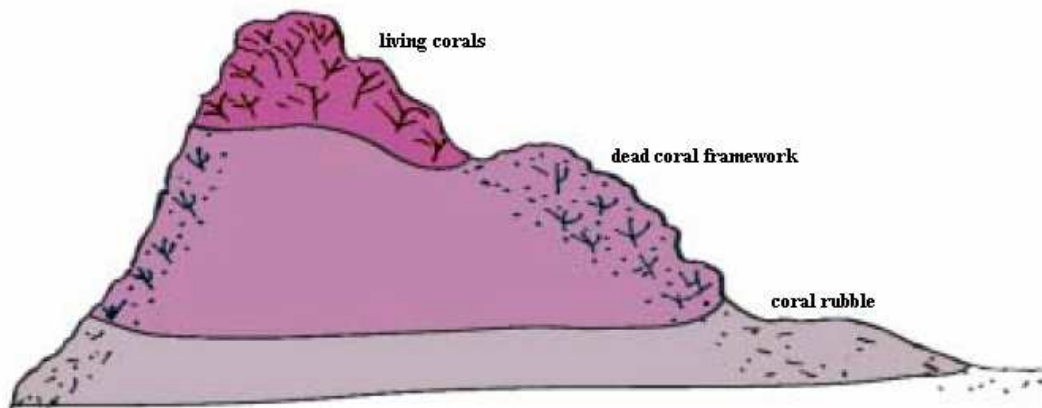


**Figure 1.2** Schematic picture of the different macrohabitats of a *Lophelia pertusa* reef. Modified from Freiwald *et al.* (2004)

The live corals are found on top of the slope or mound and show the lowest diversity because the polyps protect living tissue against predators and epifauna (Freiwald *et al.* 2004, Roberts *et al.* 2009, Rogers 1999). However, parasites like the foram *Hyrrokin sarcophaga* infest living coral polyps (Roberts *et al.* 2009, Rogers 1999). Within the living corals some mobile organisms can be found like fish, brittle stars and crustaceans (Freiwald *et al.* 2004). The mutualistic symbiont *Eunice norvegicus*, a polychaete, is the most associated species at North Atlantic *L. pertusa* reefs (Freiwald *et al.* 2004, Roberts *et al.* 2006, Roberts *et al.* 2009, Rogers 1999). The worm protects the polyps energetically against predators and the coral calcifies the parchment-like tubes which in turn stabilize the whole framework (Freiwald *et al.* 2004, Roberts *et al.* 2009).

The dead coral framework follows the living summit down slope and reveals the highest species richness (Freiwald *et al.* 2004). Octocorallia like gorgonians as well as actinians are found in this zone but also sponges, brittle stars, sea urchins, bryozoans, barnacles, and numerous worms (Freiwald *et al.* 2004, Roberts *et al.* 2009, Rogers 1999). This section constitutes the major part of a reef but it is affected by increasing sediment accumulation and bioerosion (Freiwald *et al.* 2004, Roberts *et al.* 2009, Rogers 1999).

The most degraded state, the coral rubble, forms the base of the slope or mound (Freiwald *et al.* 2004, Roberts *et al.* 2009). Coral rubble as well as broken parts of the framework create new hard substratum for further settlement or they are eroded to sediment by boring organisms, mainly sponges and fungi (see following chapter) (Roberts *et al.* 2006, Roberts *et al.* 2009, Rogers 1999). The bioeroded framework is also the habitat of encrusting sponges and echiuran worms (Freiwald *et al.* 2004, Roberts *et al.* 2009, Rogers 1999).

### 1.5.3 Bioerosion

Bioerosion can be described as the disintegration process of hard substrates like calcareous skeletons and carbonate sediments through organisms. This destructive process can be achieved by mechanical removal (bioabrasion) or by chemical dissolution (biocorrosion) or a combination of both resulting in the breakdown of substrates to smaller grains, even to silt fraction, and collapse of the framework (Beuck and Freiwald 2005, Freiwald *et al.* 2004, Roberts *et al.* 2009, Rogers 1999). Bioerosion weakens the corals and generates characteristic traces on the skeleton such as grazing marks, scars from attached organisms, excavations and borings (Roberts *et al.* 2009, Rogers 1999). Following eroding groups are found on *L. pertusa*: Bacteria, Fungi, Bryozoa, Foraminifera and Porifera (Beuck and Freiwald 2005, Bromley 2005, Freiwald *et al.* 2004). But also traces of echinoids, bivalves, and polychaetes are found (Bromley 2005).

Bioerosion affects only bare parts of the skeleton and thus the highest bioerosion rate is observed at corals which recently died (Beuck and Freiwald 2005, Bromley 2005, Freiwald *et al.* 2004, Rogers 1999). The disintegration process starts with the infestation of bacteria and fungi (Beuck and Freiwald 2005, Bromley 2005). Moreover, dead exposed framework is encrusted by bryozoans, serpulids, and bivalves (Beuck and Freiwald 2005).

Very common species eroding framework of *Lophelia pertusa* are the fungus *Dodgella* sp., the parasitic foram *Hyrrokin sarcophaga* as well as different sponges like *Alectona*

*millari*, *Spiroxya heteroclite*, *Cliona vastifica*, and *Aka labyrinthica* (Beuck and Freiwald 2005, Bromley 2005, Roberts *et al.* 2009, Rogers 1999).

### 1.6 Threats to reef structures

The relatively slow growth makes the reefs highly vulnerable to physical damage and limits recovery (Freiwald *et al.* 2004, Rogers 1999, Turley *et al.* 2007). The most surveys undertaken showed damaged or even destroyed reef structures mostly caused by deep sea fishing (Freiwald *et al.* 2004, Roberts *et al.* 2009, Rogers 1999, Rogers 2004, Turley *et al.* 2007). But there are several other aspects threatening the reefs like seabed mining, pollution, waste dumping, coral exploitation and trade as well as destructive scientific sampling and ocean acidification (see following chapter).

The most severe threat is probably bottom trawling leaving trawling scars and coral rubble behind (Freiwald *et al.* 2004, Roberts *et al.* 2009, Rogers 1999, Rogers 2004, Turley *et al.* 2007). It is assumed that 30-50 % of the Norwegian reefs are damaged by trawling (Roberts *et al.* 2009). Dragging of the heavy gear over the seabed and coral reefs leads to direct damage by flattening of coral features (Freiwald *et al.* 2004, Roberts *et al.* 2009, Rogers 1999, Rogers 2004). Reefs are damaged indirectly by higher sedimentation, redistribution of substrate but also by removal of predators (Freiwald *et al.* 2004, Roberts *et al.* 2009, Rogers 1999, Rogers 2004).

The same is true for oil and gas exploitation as well as placement of cables and pipelines. The installation of oil platforms, cables, and pipelines can damage the reef directly by placing them at or near reefs or indirectly by suspending sediment due to drill cuttings which bury the corals (Freiwald *et al.* 2004, Roberts *et al.* 2006, Roberts *et al.* 2009, Rogers 1999, Turley *et al.* 2007). Although corals use platform legs as substratum reduced growth and physiological effects, concerning metabolism and reproduction, were reported due to drill fluids (Rogers 1999).

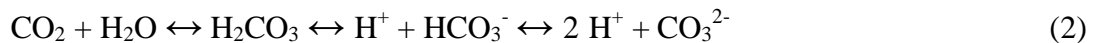
### 1.7 Climate change and ocean acidification

Although the impacts of climate change on cold-water corals are still poorly understood two features affect deep-water corals directly: rising seawater temperatures due to climate change and ocean acidification (Guinotte *et al.* 2006, Roberts *et al.* 2009).

The anthropogenic warming can be traced to 700 m water depth (Barnett *et al.* 2005) and so already threatens cold-water coral habitats.

Quite numerous studies point out that cold-water corals are highly vulnerable to changes in temperature (CSA International, Inc. 2007, Dodds *et al.* 2007, Pörtner 2008) leading to a rise in metabolism which has to be compensated by high food supply (Dodds 2007, Roberts *et al.* 2009).

Climate change and ocean acidification are coupled effects (for example Cohen and Holcomb 2009b, Fabry *et al.* 2009, Riebesell *et al.* 2000, Silverman *et al.* 2007a). Today, the ocean has absorbed one third of the anthropogenic CO<sub>2</sub> released by burning fossil fuels, cement production, agricultural practise, and deforestation (for example Feely *et al.* 2004, Orr *et al.* 2005b, Raven *et al.* 2005, Schubert *et al.* 2006). This CO<sub>2</sub> increase changes the water chemistry especially the carbonate buffer system and pH (for example Cicerone *et al.* 2004, IPCC 2007, Orr *et al.* 2005b). This buffer system can be characterized by following equation:



Increase in CO<sub>2</sub> leads to rising concentrations of H<sup>+</sup> ions which reduce pH and result also in a decline in the content of CO<sub>3</sub><sup>2-</sup> ions. Figure 1.3 describes the relationship between the species of the carbonate buffer system as well as the pH values in past and predicted.

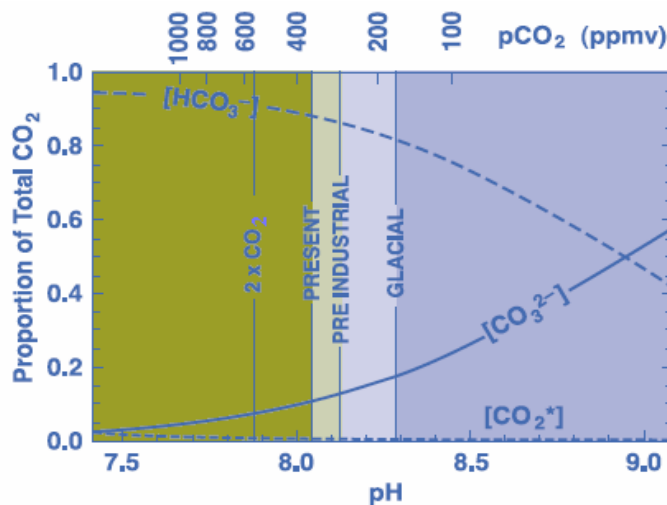


**Figure 1.3** Graph showing relative changes in inorganic carbon species in response to changes in atmospheric CO<sub>2</sub> concentrations. The values of pH for glacial and the pre-industrial period are shown as well as present and predicted levels for twice pre-industrial pCO<sub>2</sub>. From Buddemeier *et al.* (2004)

The global pH has already decreased by 0.1 units compared to the pre-industrial level (for example Feely *et al.* 2004, IPCC 2007, Orr *et al.* 2005b, Raven *et al.* 2005). A drop of 0.1 units corresponds to a 30 % increase of H<sup>+</sup> ions that means the ocean becomes more acidic (Feely *et al.* 2004, IPCC 2007, Orr *et al.* 2005b). If the trend of CO<sub>2</sub> emissions continues, there will be a decline of the pH of further 0.4 units by 2100 (for example Caldeira and Wicket 2003, Feely *et al.* 2004, Orr *et al.* 2005b, Raven *et al.* 2005).

The altered water chemistry shows impacts on physiology, growth and calcification of corals and other calcifying organisms (for example Buddemeier *et al.* 2004, Kleypas *et al.* 2006, Marubini *et al.* 2008, Raven *et al.* 2005, Riebesell 2004, Schubert *et al.* 2006).

The skeleton of corals is made of aragonite, the thermodynamically less stable form of calcium carbonate; consequently it is strongly affected by dissolution. Rising pressure and decreasing temperature with increasing depth lead to rising solubility (Raven *et al.* 2005, Schubert *et al.* 2006). Therefore, dissolution is pronounced especially in the deep ocean where it is undersaturated with respect to aragonite. In addition, deeper water already has low pH values because higher concentrations of CO<sub>2</sub> exist due to the remineralization of sinking material from the surface and respiration of benthic organisms (Feely *et al.* 2004, Raven *et al.* 2005). The older the water masses the more they are enriched in CO<sub>2</sub> resulting in undersaturation at certain depth.

This depth at which aragonite begins to dissolve is termed aragonite saturation horizon (ASH) and can also be defined as the boundary between over- and undersaturation. The ASH is shallower in the Pacific than in the Atlantic Ocean since the conveyor belt transports water masses from the Atlantic to the Pacific (Feely *et al.* 2004, Orr *et al.* 2005b). So the water is old and CO<sub>2</sub>-enriched in the Pacific (Feely *et al.* 2004, Orr *et al.* 2005b). The saturation horizon of aragonite is 200-1000 m in the North Pacific (Feely *et al.* 2004) and > 2000 m in the Atlantic (Figure 1.4) (Guinotte *et al.* 2006). The ASH, however, is rising due to acidification because of increasing CO<sub>2</sub> concentration (for example Feely *et al.* 2004, Orr *et al.* 2005b). The ASH is approximately 200 m shallower compared to that of the pre-industrial period (for example Feely *et al.* 2004, Guinotte *et al.* 2006, Raven *et al.* 2005, Schubert *et al.* 2006). Moreover, Orr *et al.* (2005b) predicts that the ASH will rise to about 100 m in the North Atlantic by 2100 under the IPCC IS92a, business as usual, scenario.

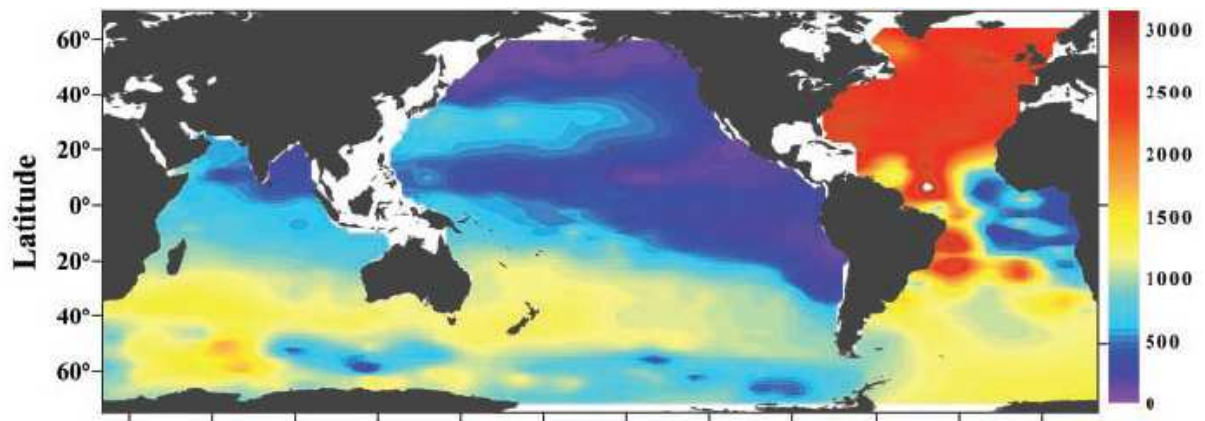


**Figure 1.4** Distribution of aragonite saturation horizon in the global oceans showing the shallow ASH in the Pacific Ocean and the deep saturation horizon in the North Atlantic. The pressure effect on the solubility was estimated from the equation of Mucci that included the adjustments to the constants recommended by Millero. From Feely *et al.* (2004)

Several studies point out that the distribution of cold-water coral reefs is limited to saturated waters with respect to aragonite (Davies *et al.* 2008, Guinotte *et al.* 2006, Roberts *et al.* 2006). To date, no stony coral reefs, comparable to those in the North Atlantic, were found in the North Pacific (Guinotte *et al.* 2006, Roberts *et al.* 2006). North Pacific reefs are dominated by soft corals, gorgonians and lace corals (Roberts *et al.* 2006). This lack of reef frameworks in the North Pacific could be attributed to the shallower ASH (Guinotte *et al.* 2006, Roberts *et al.* 2006). Moreover, it is expected that more than 70 % of the deep-sea reefs will be undersaturated by 2100 (Guinotte *et al.* 2006, Roberts *et al.* 2009); assuming 788 ppm CO<sub>2</sub> by 2100 according to the IPCC IS92a scenario (Turley *et al.* 2007, Turley 2008). However, some reefs will already experience undersaturation as early as 2020 (Guinotte *et al.* 2006, Turley *et al.* 2007, Turley 2008).

As mentioned before, rising pCO<sub>2</sub> leads to undersaturation of CaCO<sub>3</sub> resulting in dissolution of calcareous coral skeletons (for example Kleypas *et al.* 2006, Raven *et al.* 2005, Riebesell *et al.* 2009, Schubert *et al.* 2006). Dissolving of CaCO<sub>3</sub> leads to increases in the concentrations of inorganic carbon species in seawater (see reversed equation 1). This rise can easily be determined by means of total alkalinity.

Total alkalinity (TA) can be defined as the amount of protons required for neutralising all anions in a seawater sample and can be described by following equation:

$$\text{TA} = [\text{HCO}_3^-] + 2 [\text{CO}_3^{2-}] + [\text{B}(\text{OH})_4^-] + [\text{OH}^-] - [\text{H}^+] + [\text{HPO}_4^{2-}] + 2 [\text{PO}_4^{3-}] + [\text{NH}_3] + [\text{H}_3\text{SiO}(\text{OH})_3^-] + [\text{HS}^-] - [\text{H}_3\text{PO}_4] - [\text{HSO}_4^-] - [\text{HF}] \quad (3)$$

where terms in brackets stand for the concentration of these ions and molecules in seawater (Dickson *et al.* 2007). The concentrations of  $\text{NH}_3$  and  $\text{HS}^-$  are low in open ocean water thus they can be neglected (Dickson *et al.* 2007). Furthermore, the concentrations of conservative elements like borate, fluoride, and sulphate can be calculated via the salinity of the seawater sample (Schulz *et al.* 2009). In general, TA reflects the amount of carbonate ion species because carbonate and bicarbonate ions contribute the major portion to total alkalinity. Therefore, any variations in the concentration of dissolved inorganic carbon due to calcification or dissolution are shown in alkalinity changes. However, solving of  $\text{CO}_2$  in seawater, release of  $\text{CO}_2$  to the atmosphere as well as photosynthesis and respiration have no impact on TA.

Another important parameter describing ocean water chemistry is the aragonite saturation state ( $\Omega_{\text{Ar}}$ ) which expresses the  $\text{CO}_3^{2-}$  ion concentration in the water column and can be defined by following equation:

$$\Omega_{\text{Ar}} = \frac{[\text{Ca}^{2+}][\text{CO}_3^{2-}]}{K'_{\text{sp}}} \quad (4)$$

where  $[\text{Ca}^{2+}]$  and  $[\text{CO}_3^{2-}]$  are the concentrations of calcium and carbonate ions, respectively and  $K'_{\text{sp}}$  is the stoichiometric solubility product of aragonite at given temperature, salinity, and pressure. When  $\Omega_{\text{Ar}} > 1$  the water is oversaturated with respect to aragonite and at  $\Omega_{\text{Ar}} = 1$  the concentrations of the ions are in equilibrium. At  $\Omega_{\text{Ar}} < 1$  the water is undersaturated with respect to aragonite resulting in a decline in coral calcification and in an increase in dissolution of the skeleton as mentioned before (for example Buddemeier *et al.* 2004, Feely *et al.* 2004, Kleypas *et al.* 2006, Raven *et al.* 2005, Schubert *et al.* 2006). Due to ocean acidification the aragonite saturation state is declining because of decreasing  $\text{CO}_3^{2-}$  ion concentrations leading to limited habitat suitable for marine



calcifiers using aragonite (Figure 1.5) (for example Caldeira 2007, Feely *et al.* 2009, Raven *et al.* 2005, Turley 2008).

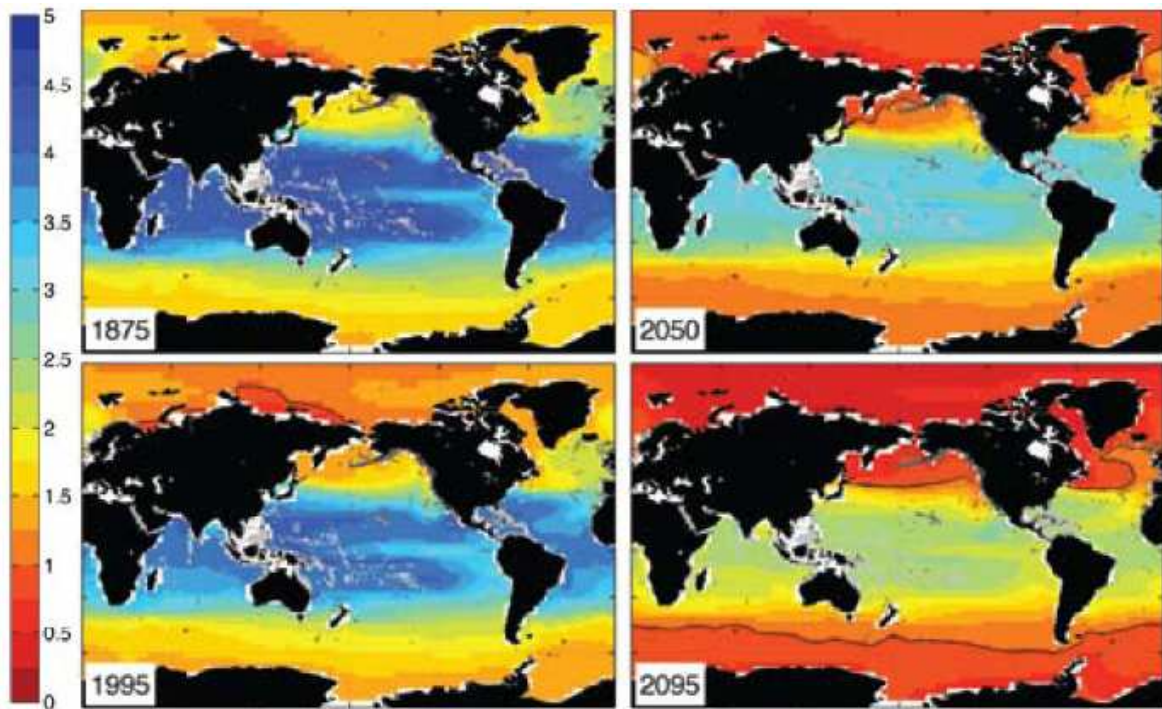


**Figure 1.5** Maps illustrating the decline in  $\Omega_{Ar}$  in the global oceans. CCSM3-modeled decadal mean  $\Omega_{Ar}$  at sea surface, centred around the years 1875, 1995, 2050, and 2095. From Feely *et al.* (2009)

Climate change and ocean acidification are coupled phenomena so it is difficult to divide them into separate effects (Feely *et al.* 2004, Raven *et al.* 2005, Silverman *et al.* 2007a). Those effects could have great impacts on the entire ecosystem by changing water mass characteristics or species interactions (Buddemeier *et al.* 2004, Hoegh-Guldberg *et al.* 2007, Kleypas *et al.* 2006, Riebesell *et al.* 2007, Wootton *et al.* 2008). Therefore, severe ecosystem impacts are very likely (Kleypas and Langdon 2006). If reefs were dissolving the ecosystem will change towards lower complexity, diversity, and resilience (Caldeira 2007) which means the habitat could be lost for associated fauna concerning the bioengineer functions like providing habitat, food and nursery (Maynard *et al.* 2008d). Additionally, the whole food web may be affected, for example, by desynchronising hatching of zooplankton larvae at times of phytoplankton blooms resulting in alterations in nutrient and food supply for corals (Feely *et al.* 2004, Kleypas *et al.* 2006, Raven *et al.* 2005).

On the other hand, respiration rates of corals but also that of endolithic and encrusting organisms would increase due to rising temperatures which could lead to higher bioerosion rates and therefore enhanced dissolution (Andersson *et al.* 2009, Silverman *et al.* 2007a). It is also unclear if the corals will be more susceptible towards pathogens and parasites like tropical coral species (Roberts *et al.* 2009).

Additionally, coral skeletons are likely to become less dense due to dissolution which may reduce the resistance to breakage and bioerosion and the ability of competition could decrease (Andersson *et al.* 2008, Buddemeier *et al.* 2004, Schubert *et al.* 2006). But declining calcification rates and dissolution may occur even before the water is undersaturated; if cold-water corals reacted the same way like their tropical counterparts (Cohen *et al.* 2009a, Turley *et al.* 2007). A lower pH and lower  $\Omega_{Ar}$  imply that corals require more energy for calcification which means less energy is available for metabolism, growth and fitness (Andersson *et al.* 2008, Cohen and Holcomb 2009b, Maynard *et al.* 2008d). Other physiological effects could be an acidification of body fluids (Marubini *et al.* 2008) affecting oxygen supply (Dodds *et al.* 2007, Pörtner 2008), egg production, recruitment and genetic diversity (Andersson *et al.* 2009, Cohen and Holcomb 2009b).

All these accumulating effects raise the question whether corals are able to adapt to changing environment. Corals may adapt to local conditions (Maynard *et al.* 2008d), on longer time scales (Buddemeier and Smith 1999a) or might migrate towards higher latitudes concerning temperature rises or towards shallower waters because of shoaling of the aragonite saturation horizon (Andersson *et al.* 2008). Therefore, corals may not become distinct. It was suggested that they could survive without their skeleton (Hoegh-Guldberg *et al.* 2007, Pörtner 2008) or may shift their mineral type (Andersson *et al.* 2008, Kleypas and Langdon 2006). However, adaptation remains unclear because of uncertainties in physiological stress responses, reproduction strategies as well as calcification process (Buddemeier and Smith 1999a). Moreover, the rise in CO<sub>2</sub> occurs too fast for adaptation (for example Buddemeier and Smith 1999a, Caldeira 2007, Freiwald *et al.* 2004, Kleypas *et al.* 2006, Raven *et al.* 2005), especially cold-water corals may have less time for generations to accommodate due to slow growth and low metabolism (Fabry *et al.* 2009).

## 1.8 Skeletal characterisation

### 1.8.1 Structure

Aragonite is one mineral type of  $\text{CaCO}_3$  revealing an orthorhombic crystal structure. The mineral is physically stronger but thermodynamically less stable than calcite, another mineral form of calcium carbonate.

In general, the aragonite crystals are several  $\mu\text{m}$  in length,  $0.5\text{-}1\ \mu\text{m}$  wide and are tightly packed into bundles (Cohen and Holcomb 2009b).

Crystal morphology depends on  $\Omega_{\text{Ar}}$ , organisation and packing of the crystals (Cohen and Holcomb 2009b). When  $\Omega_{\text{Ar}}$  is high, crystals are long, thin, needle-like, and fast growing but crystals are short, wide, faceted, not oriented in bundles, and exhibit slower growth rates when  $\Omega_{\text{Ar}}$  is low (Figure 1.6) (Cohen and Holcomb 2009b).

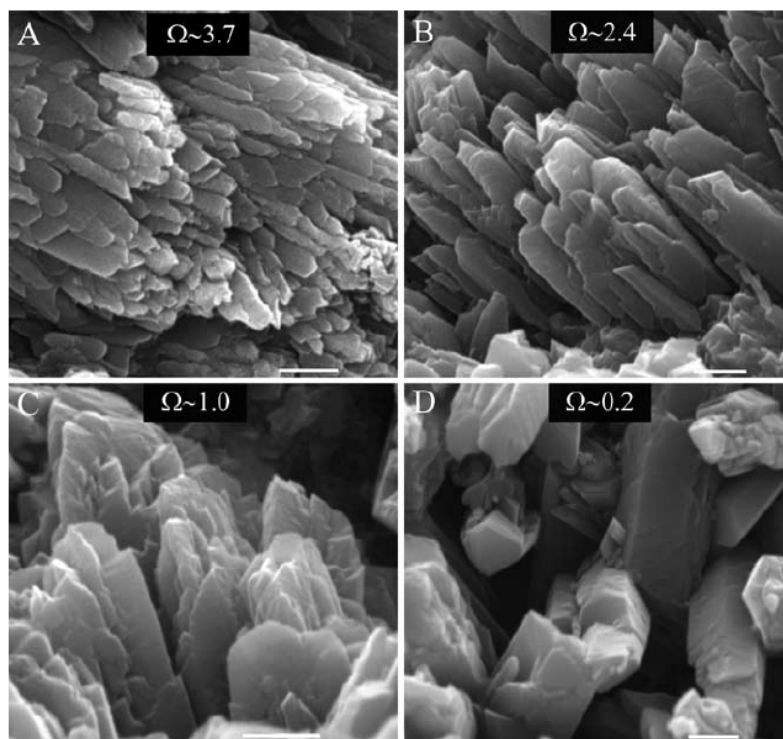


**Figure 1.6** Scanning electron microscopy (SEM) images showing aragonite crystals accreted by corals, reared in seawater with given ranges of  $\Omega_{\text{Ar}}$  (A-D). Images reveal changes in aragonite structure due to acidification resulting in changes of crystals in size, shape, orientation, and composition. From Cohen *et al.* (2009a)

### 1.8.2 Composition

The coral skeleton consists of aragonite mineral and an organic matrix (for example Allemand *et al.* 2004, Cohen *et al.* 2006, Cuif *et al.* 2004a, Dauphin *et al.* 2008). Studies showed that this organic matrix at which calcification takes place is a proteoglycan matrix

and the organic material found within the skeleton seems to be comprised of acidic sulphated polysaccharides, sugars and proteins (Cuif and Dauphin 2005b, Dauphin *et al.* 2008, Puvarel *et al.* 2005b). The amount of this organic material was documented to be in the order of 0.1-1 % of dry weight (Allemand *et al.* 2004, Gaffey *et al.* 1991). Although this organic fraction is very small it is important for crystal nucleation and is deposited simultaneously with the mineral and not sequentially as thought before (Allemand *et al.* 2004). The highest portion of organic molecules was found near the centres of calcification (Cuif and Dauphin 2005b).

The composition of the organic material seems to depend on taxonomy resulting in species-specific crystals and skeletal architecture (Cuif and Dauphin 2005b, Dauphin *et al.* 2006). This compositional variability could arise from combined alterations in water temperature and seasonal changes in the mass of aragonite precipitated (Cohen *et al.* 2006).

### 1.8.3 Comparison between biogenic and abiogenic aragonite

Abiogenic aragonite only precipitates spontaneously at high aragonite saturation states whereas corals can elevate their internal  $\Omega_{Ar}$  for biomineralization (see chapter 1.4.4 Biomineralization) (Cohen and Holcomb 2009b, Kleypas and Langdon 2006). Abiogenic aragonite crystals show similar organisation to crystals formed by corals (Cohen and Holcomb 2009b). Biogenic and abiogenic aragonite can also be compared by their temperature of thermal degradation being 550°C for coral carbonates whereas pure aragonite was stable until 600°C (Cuif *et al.* 2004a). Furthermore, the temperature range for conversion of aragonite into calcite seems to be lower for the biogenic aragonite than for the abiogenic one (Dauphin *et al.* 2006).

Biogenic aragonite has another composition than pure aragonite including further elements like Sr, Mg, S, C and Si (Cohen *et al.* 2006, Cuif and Dauphin 2005b, Gaffey *et al.* 1991, Meibom *et al.* 2007, Zhong and Mucci 1989). The biogenic aragonite is formed by means of an organic matrix under biologically controlled conditions (Cuif *et al.* 2004a, Cuif and Dauphin 2005b, Marubini *et al.* 2008, Meibom *et al.* 2007). In experiments, Cohen *et al.* (2006) plotted Sr/Ca ratios against temperature and received different slopes of regression lines for distinct coral species and abiogenic aragonite. These relative changes in isotopic values could be caused by changes in seawater temperature, its isotopic composition (Cohen *et al.* 2006) or by variations in biological processes (Blamart *et al.* 2007).

Furthermore, the density of coral skeletons is different from pure aragonite due to the organic compounds or distinct crystal lattice (CSA International, Inc. 2007, Dodds 2007, Hughes 1987). The density of pure aragonite is 2.93 g/ cm<sup>3</sup> (Weast and Astle 1980). Deviations from the pure mineral may be affected by pH, nutrients, and current speed (CSA International, Inc. 2007, Dodds 2007) beside different composition.

### 1.9 Dissolution kinetics

The formation of carbonates is influenced by thermodynamic kinetics (Zhong and Mucci 1989). Near equilibrium, when  $\Omega_{Ar} = 1$ , the dissolution is mostly surface-controlled which means the surface structure of the skeleton controls how effectively corrosive water can attack and thus dissolution behaves non-linear with respect to  $\Omega_{Ar}$  (Morse and Arvidson 2002b). When  $\Omega_{Ar}$ , however, is far from equilibrium dissolution became diffusion-controlled depending on how many corrosive-acting molecules are near the skeleton surface and then dissolution is linear with respect to  $\Omega_{Ar}$  (Morse and Arvidson 2002b). Therefore, dissolution results in saturation curves with a sharp increase under highly undersaturated conditions forming a plateau when saturation is reached near the equilibrium.

Numerous examinations has been carried out about dissolution kinetics and the behaviour of carbonates in undersaturated water mostly during the late 60s and 70s (Berger 1967, Berner and Wilde 1972, Keir 1979, Morse *et al.* 1979, Morse and Berner 1972, Peterson 1966, Walter and Morse 1985, Zhong and Mucci 1989). Such dissolution experiments, however, showed different results due to disagreement on the solubility constants and methods applied (Berner *et al.* 1976, Honjo and Erez 1979, Keir 1979). It was found that dissolution occurs at various depths due to degree of undersaturation (Milliman 1975, Berger 1967) and current flow which provides the sample with fresh corrosive water (Berger 1967). Moreover, dissolution removes carbonate layer-by-layer so there is not much damage visible but the material becomes increasingly thinner (Berger 1967). This layer-by-layer removal could explain why dissolution rates ceases with time under natural conditions because the most susceptible parts vanish first (Berger 1967).

In general, dissolution depends on surface texture and composition (Morse and Arvidson 2002b, Morse and Berner 1972) meaning the microstructure, mineral stability (Walter and Morse 1985) as well as surface to volume ratio (Morse and Arvidson 2002b). Biogenic

carbonates dissolves at lower rates than abiogenic ones maybe due to less surface area presented to undersaturated water (Morse *et al.* 1979, Walter and Morse 1985) or less reactive surface area (Walter and Morse 1985). In experiments, foram tests dissolved faster after initial solution probably caused by increased surface area available for dissolution (Morse *et al.* 1979). Additionally, bleached samples were more vulnerable than untreated samples (Berger 1967, Honjo and Erez 1979).

### 1.10 Thesis outline

A few studies have been carried out about skeleton structure and composition of *Lophelia pertusa* (Blamart *et al.* 2007, Cohen *et al.* 2006, CSA International, Inc. 2007, Cuif *et al.* 2004a, Cuif and Dauphin 2005b). But to date, no data exist at which aragonite saturation state *L. pertusa* skeletons starts to dissolve.

Knowledge of the critical  $\Omega_{Ar}$  would be an advantage in predicting the impacts on cold-water corals concerning raising aragonite saturation horizon due to ocean acidification. Moreover,  $\Omega_{Ar}$  given in literature always refers to the pure mineral aragonite. But it was found that the skeleton of *L. pertusa* had a lower density, and thus probable different  $\Omega_{Ar}$ , than pure aragonite (CSA International, Inc. 2007). This difference could possibly arise due to organic compounds or different crystal lattice (CSA International, Inc. 2007) which could explain the ability of calcification at  $\Omega_{Ar} \leq 1$  (Cohen *et al.* 2009a, Form and Riebesell submitted, Maier *et al.* 2009). Furthermore, it seems likely that the critical aragonite saturation state is species-specific (Cuif and Dauphin 2005b, Honjo and Erez 1979) which means that the identified value is not representative for cold-water corals in general.

The aim of this diploma thesis was to find the critical  $\Omega_{Ar}$  of dead skeletons by investigating coral fragments under different pCO<sub>2</sub> treatments. The hypothesis of the diploma thesis was that skeletons of *Lophelia pertusa* will start to dissolve at an  $\Omega_{Ar} < 1$ . Therefore, H<sub>0</sub> was that dissolution started at or above the value 1.

To determine that particular  $\Omega_{Ar}$ , pH and total alkalinity were measured. Total alkalinity showed changes in water carbonate chemistry because carbonate ion species were released by dissolution of coral skeletons (see chapter 1.7 Climate change and ocean acidification). Moreover, alkalinity can easily be measured and provides accurate values.

Two sets of experiments were implemented. In the main experiment coral skeleton fragments were exposed to seawater with different  $p\text{CO}_2$  values with respect to  $\Omega_{\text{Ar}}$ . The  $p\text{CO}_2$  values chosen referred to  $\Omega_{\text{Ar}} > 1$ , near equilibrium which means  $\Omega_{\text{Ar}} \approx 1$ , and values well below 1. According to dissolution kinetics saturation curves (one for each treatment) were expected which then illustrated the critical saturation state for *Lophelia pertusa*. The second experiment was carried out similar to the first one but only one high  $p\text{CO}_2$  value was selected for fast reaction and saturation response. Samples in this control experiment were treated prior the dissolution experiment by removing all organic material on the outside of the skeletons by sterilizing and bleaching. This control experiment was supposed to show potentially changes between both approaches.

Additionally, scanning electron microscopy images were taken after the completion of the main experiment to investigate visible dissolution effects on the outer wall of calices as well as on septa.

Furthermore, ash-free dry weights of skeleton were examined to determine the organic fraction within skeleton by means of combustion.

## 2. Materials and Methods

The parameters regularly measured were pH, dissolved inorganic carbon (DIC) and total alkalinity (TA). Before starting the experiments, nutrients were measured (nitrate, total phosphate, silicate) to take them into account for the carbonate system because they can alter alkalinity (Zeebe and Wolf-Gladrow 2001, Gattuso *et al.* 2010). Since initial nutrient measurements revealed significant low values they were neglected for further calculations (see table in Appendix).

Bottles with a capacity of 0.5 l (Duran Schott) were used in the experiments and caps were screwed air-tight to avoid outgasing of CO<sub>2</sub>. The bottles were stored at 15 ± 1°C in a temperature chamber at the IFM-GEOMAR. The bottles were stirred daily to maintain homogenous conditions avoiding the formation of gradients within the bottles.

Reproducibility was guaranteed by carefully preparing the material for the experiments which involved filtering natural seawater (NSW), cleaning of corals, handling all treatments equally as well as regularly measuring the parameters to recognize possible shifts.

### 2.1 Main experiment

This experiment was carried out in bottles containing manipulated water with different pCO<sub>2</sub> values achieved by acidification.

The 0.5 l bottles (Duran Schott) used were autoclaved prior experiment. Sealed coral fragments (see details about sealing in chapter 2.2.3 Coral material) were weighed to 0.01 g (Sartorius LA 2200P, accuracy: ± 0.01 g), the average weight of the material was 66.64 ± 0.04 g.

Filtered NSW (salinity: 33.6) was manipulated in 10 l plastic water canisters, one for each treatment (see chapter 2.2.2 Acidification). The canisters were weighed to the nearest 0.1 g (Sartorius CPA 34001S, accuracy: ± 0.1 g). The bottles were rinsed with the acidified water before they were completely filled with that water. Each bottle of the respective pCO<sub>2</sub> treatment contained the same water.

The pCO<sub>2</sub> values selected referred to the aragonite saturation state. Treatments chosen were: control (non-manipulated water), 1200, 1800, and 2500 ppm CO<sub>2</sub> which correspond to  $\Omega_{Ar}$  of 2.14, 1.02, 0.71, and 0.53, respectively. The number of replicates for each treatment was n = 7 and n = 5 for the control. Additionally, one blank for each treatment was prepared without coral material containing the corresponding acidified seawater.



The experimental set-up is shown in Figure 2.1.

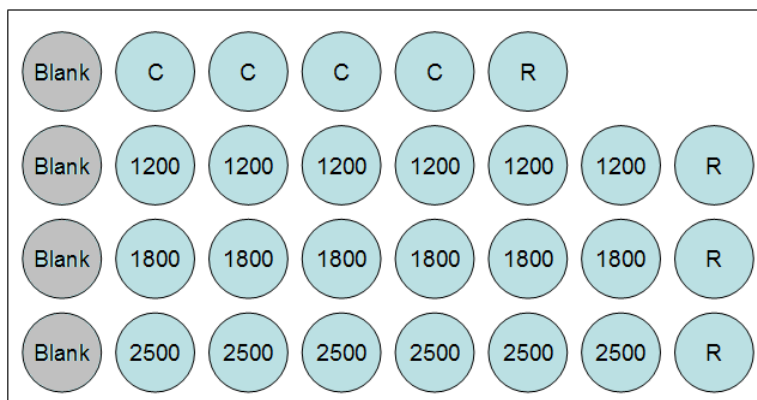


**Figure 2.1** Diagram presenting the experimental set-up. One blank for each treatment and one for the control (C), respectively. Number of replicates were  $n = 7$  for the  $p\text{CO}_2$  treatments (1200, 1800, 2500 ppm  $\text{CO}_2$ ) and  $n = 5$  for the control containing ambient seawater. Seventh bottle first opened at day 36 acting as reserve (R) (see explanation in text).

Coral fragments were added to each bottle and poisoned with  $150 \mu\text{l HgCl}_2$  (dilution ratio: 1:4800) and stored and handled as mentioned above. The first six treatment bottles were sampled; one bottle of each treatment was taken each sampling day to diminish outgasing via growing headspace within the bottles. In this way, the first bottle was measured again after six sampling days. Samples were taken every two days for the first 12 days and then after four days until day 36. The seventh bottle (reserve) was sampled at the end of the experiment (day 36), when measurements of alkalinity indicated saturation. Therefore, end point samples were measured without prior opening. The last sampling took place on day 50 and was a re-measurement of the reserve.

Samples were taken by use of a 100 ml syringe (Braun Omnifix, sterile-EO) and filled into 60 ml glass vials. The vials were sealed with glass stoppers without leaving headspace and were stored at  $15^\circ\text{C}$  until measurement. Since the measuring method of total alkalinity and pH was performed at standard temperature of  $20^\circ\text{C}$  samples were kept in a water bath at  $20 \pm 1^\circ\text{C}$  for equilibration prior analysis. First, samples for DIC were taken followed by pH measurement and then total alkalinity was determined (see measuring procedures in chapter 2.6 Measurements).

## 2.2 Media preparation

### 2.2.1 Water filtration

Natural seawater from the North Atlantic (POS 391 cruise) with a salinity of 33 was filtered through a 0.2 µm filter capsule (Polycap 75 AS, sterile and non-pyrogenic). The water was filtered to eliminate particles or algae growing in the water tank used.

### 2.2.2 Acidification

The pCO<sub>2</sub> concentrations for the treatments were chosen with respect to the aragonite saturation state. Acidification of the seawater was achieved by adding HCl to obtain predefined pCO<sub>2</sub> values (Gattuso *et al.* 2010, Schulz *et al.* 2009). Na<sub>2</sub>CO<sub>3</sub> was added afterwards to restore alkalinity to the initial value according to Schulz *et al.* (2009) and Gattuso *et al.* (2010).

Na<sub>2</sub>CO<sub>3</sub> (Merck, suprapur, Germany) and 3.571 M HCl (Merck, Germany) were used for the manipulation of the seawater.

Before starting an experiment, fresh stock solution of combusted Na<sub>2</sub>CO<sub>3</sub> was prepared. Each bottle was acidified according to treatment pCO<sub>2</sub> values in the test run I (see chapter 2.3.1 Test run I). For the main experiment 10 l plastic water canisters, one for each treatment, were filled with filtered NSW without headspace and manipulated accordingly (see further details on acidification in Appendix).

### 2.2.3 Coral material

Skeletal material of *Lophelia pertusa* was sampled at the Oslo Fjord during the AL 275 cruise in 2006 (59°04' N, 10°46' E; depth: 80-150 m). Furthermore, corals from the Sula Reef were collected during the AL 316 cruise in 2008 (64°05' N, 8°0' E; depth: 275-300 m) and the POS 391 cruise in 2009 including the polar reef LoppHAVet (70°25' N, 21°10' E; depth: 225-270 m). Locations of the sampling sites are shown in Figure 2.2. For detailed information about sampling the reader is referred to the scientific cruise reports.

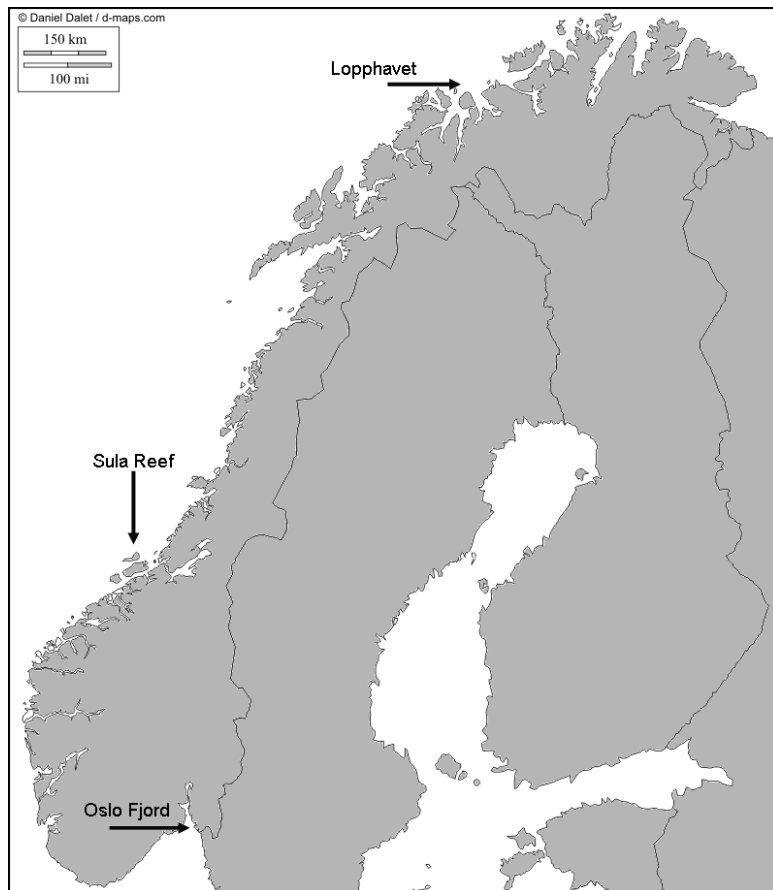


**Figure 2.2** Map of the locations of sampled coral reefs.

For the experiments coral material was selected randomly assuming a good mixture of samples from all sites.

The white colour variety was used for the manipulation experiments. Exclusively healthy looking parts of the colony were taken. Fragments heavily affected by bioerosion and parts overgrown by epibionts (for example brachiopods, bryozoans, and tubes of polychaetes) were excluded because boring or attached organisms have already affected the skeleton surface which in turn might change dissolution response.

At first, the skeletal material was cleaned by eliminating organic remains and tissue. However, it was not possible to remove all tissue in the calices without breaking the septa.

The breaking edges and fissures were sealed with paraffin wax to avoid dissolution of detached skeletal material. In a pre-measurement it was tested which sealing substance worked best under high  $p\text{CO}_2$  without affecting water chemistry (see chapter 2.3.2 Test run II).

### 2.3 Preliminary tests

After testing the method of experimental seawater acidification for precision different test experiments were carried out prior the main and control experiment. Test run I was a dissolution experiment with coral rubble to find out the appropriate CO<sub>2</sub> concentrations for the main experiment. In test run II different substances were tested for sealing breaking edges and fissures of the coral fragments without altering water chemistry. In test run III several chemicals were examined to ensure constant conditions for the main and control experiment concerning possible biological activity by micro-organisms which could influence measured parameters. In test run IV further coral material was tested to define stable control conditions. To achieve such stable conditions coral material was bleached and sterilised to remove any remaining tissue as well as eliminate possible existing micro-organisms.

#### 2.3.1 Test run I: Dissolution experiment with coral rubble

This test run was carried out with cleaned and dried coral rubble without paraffin sealing. The experiment was performed in 0.5 l bottles (Duran Schott) filled with filtered NSW and stored and handled as mentioned before. Different pCO<sub>2</sub> concentrations for the treatments were chosen with respect to the aragonite saturation state to find out the appropriate pCO<sub>2</sub> values for the main experiment. Treatments chosen were: control with ambient seawater (472.6 ppm CO<sub>2</sub>), 1200, 1400, 1600, 1800, 2000, 2200, and 2400 ppm CO<sub>2</sub>. These pCO<sub>2</sub> values correspond to  $\Omega_{Ar}$  of 2.31 for the non-manipulated water, 1.02 for 1200 ppm CO<sub>2</sub>, 0.89, 0.79, 0.71, 0.65, 0.59, and 0.55 for the other treatments, respectively. The bottles were stirred daily (see handling procedure at the beginning of this chapter). Alkalinity was examined after 7, 14, 21, and 28 days. Samples were taken with a 50 ml syringe (Infuject, sterile-R) and subsequently stored in 50 ml PP bottles with screw cap without headspace.

#### 2.3.2 Test run II: Sealing experiments

Different materials (two types of silicones, two types of wax) were tested for their magnitude of reaction with respect to alkalinity to find an appropriate sealing substance. Transparent silicone (JBL Aquasil, acetoxyl sealant, solvent free) and black silicone (Rotabond 2000, UV resistant, solvent and isocyanate free) were examined as well as two types of wax. One wax consisted of 80 % paraffin and 20 % stearin (Knorr Prandell) and the other was pure paraffin (Carl Roth GmbH & Co. KG). As a control, plastic biofilter material was used as a chemically inert substitute for coral skeleton because this material

itself did not change water chemistry. This plastic biofilter material and coral fragments were completely covered with the respective chemical substance for rapid response and kept in ambient filtered seawater.

### 2.3.3 Test run III: Elimination of possible micro-organisms

A pre-test showed a significant drop in pH indicating biological activity by micro-organisms. Therefore, corals were treated with an antibiotic and a fungicide to eliminate possible disturbing micro-organisms. The fungicide used was cycloheximide ( $C_{15}H_{23}NO_4$ ) which inhibits the protein synthesis of eukaryotic organisms. The cycloheximide had a concentration of 20.59 mg/ l. The second chemical, chloramphenicol ( $C_{11}H_{12}Cl_2N_2O_5$ ), is a broad-spectrum antibiotic that also inhibits protein synthesis; applied concentration was 50.56 mg/ l.

After that pre-treatment cycloheximide, chloramphenicol, mercury chloride, and autoclaving were tested to maintain constant conditions during experiment.

This trial included untreated corals, autoclaved corals, autoclaved + antibiotic/fungicide treated corals, not autoclaved + antibiotic/ fungicide treated corals, and corals poisoned with  $HgCl_2$ . The concentration of cycloheximide and chloramphenicol in the treatment with autoclaved material was 62 mg/ l and 84.1 mg/ l, respectively and in the treatment with non-autoclaved corals 53.4 mg/ l and 84.1 mg/ l, respectively. Each treatment was carried out in a single 0.5 l bottle (Duran Schott) filled with filtered NSW without headspace, closed air-tight, and stored at  $15 \pm 1^\circ C$ , subsequently and handled as described above. Total alkalinity and pH were measured after six days. Samples were taken similar to test run I. Since the test bottle with mercury chloride indicated constant conditions concerning pH as well as alkalinity (see chapter 3.1 Preliminary tests) the coral material used in the main experiment was kept in  $HgCl_2$  solution (dilution ratio: 1:2000) for some days and then rinsed thoroughly and dried.

### 2.3.4 Test run IV: Eliminating organic remains

Coral fragments were cleaned, bleached for 3.5 days with NaOCl (dilution ratio: 1:3) and sterilised at  $> 100^\circ C$  for 52 minutes. Afterwards, the material was rinsed thoroughly with NSW and poisoned with mercury chloride. This test was performed in a 0.5 l bottle (Duran Schott) completely filled with filtered NSW and stored and handled as mentioned before.

Samples were taken and analysed in the same manner as for the main experiment (see chapter 2.1 Main experiment). Samples were taken and analysed after 5, 10, and 30 days.

#### 2.4 Control experiment

The control experiment was performed in bottles containing manipulated water with different pCO<sub>2</sub> values achieved by acidification or bubbling with CO<sub>2</sub>-enriched air.

This experiment was carried out with autoclaved 0.5 l bottles (Duran Schott). Coral fragments were cleaned, crushed into small pieces, sterilised at > 100°C for one hour, and rinsed with NSW. The fragments were bleached with NaOCl for seven days (dilution ratio 1:4), rinsed, and sterilised again for 65 minutes. The coral pieces were rinsed thoroughly and kept seven days in seawater because a pre-test showed that total alkalinity altered after sterilisation.

The coral material was weighed wet reading to 0.01 g (Sartorius LA 2200P), the average weight was 115.91 g ± 1.61 g.

Similar to the main experiment, the pCO<sub>2</sub> value chosen referred to the aragonite saturation state. A high pCO<sub>2</sub> treatment with 2400 ppm CO<sub>2</sub> was selected as well as a control with ambient seawater. These pCO<sub>2</sub> values correspond to  $\Omega_{Ar}$  of 0.54, and 2.52, respectively. The number of replicates for the treatment was three and one for the control. One bottle of each treatment was intentionally left without coral material containing the corresponding acidified or non-manipulated seawater, respectively. These bottles served as blanks.

The coral material was divided for two different experimental set-ups. Sub-experiment one (S<sub>I</sub>) was carried out as the main experiment and in sub-experiment two (S<sub>II</sub>) the bottles were bubbled with CO<sub>2</sub>-enriched air (Figure 2.3).

The control of S<sub>II</sub> was treated with compressed air. The compressed as well as the CO<sub>2</sub>-enriched air were moisturized by means of two litres gas wash bottles (Duran Schott) and were then connected to the treatment bottles and blanks. The inflow was controlled via valves; one was used as pressure relief valve. Furthermore, one valve per bottle allowed adjusting bubbling for each bottle separately (Figure 2.3).

Filtered NSW (salinity: 33.3) for the non-bubbled bottles (S<sub>I</sub>) was manipulated in a single 10 l plastic water canister so each treatment bottle contained the same water (see details on acidification in Appendix). The bottles were rinsed with the acidified water before they were filled without headspace.

Coral fragments were added to each bottle and poisoned with 150  $\mu\text{l}$   $\text{HgCl}_2$  (dilution ratio: 1:4800). The bottles were stirred daily to avoid the formation of gradients in the water.

Experimental conditions and sampling was comparable to the main experiment concerning storage temperature as well as measuring and sampling procedure.

Samples were taken at different time intervals especially the control treatments because of limited water volume. The control of  $S_{\text{I}}$  was sampled at day 0 and then after 4, 8, 14, and 20 days. The control of  $S_{\text{II}}$  was sampled at days 0, 4, 10, and 18 and the 2400 ppm  $\text{CO}_2$  treatments after 0, 2, 4, 6, 8, 10, 14, and 18 days. Samples of the blanks were taken every six days. However, the blanks of the 2400 ppm  $\text{CO}_2$  treatment of  $S_{\text{II}}$  which had 3 blanks in total were sampled after 0, 2, 4, 6, 12, and 18 days. One of the blanks was sampled each time as in the main experiment.



**Figure 2.3** Set-up for sub-experiment two showing the 2400 ppm  $\text{CO}_2$  treatment as well as its blanks without corals (blanks in the back). Valves (black) directed to each bottle allowed adjusting of the bubbling. One valve served as pressure relief valve (arrowed). Using the two litres bottle as gas wash bottle (in the back) the air was moisturized before running to the treatment bottles.

### 2.5 Determination of organic content in coral skeleton

White coral pieces from the Sula Reef (AL 318 cruise in 2008; see details in chapter 2.2.3 Coral material) were defrosted and rinsed cautiously to preserve coral tissue within the calices. However, not all coral pieces contained remaining tissue. The fragments were weighed reading to 0.001 mg using a high precision balance (Sartorius M2P, accuracy:  $\pm 0.003$  mg). The tissue was removed and the fragments were bleached with

NaOCl (dilution ratio: 1:4). The corals were rinsed with distilled water and dried at 50°C for 24 hours. Then, the weight was measured again. The fragments were grinded (IKA mortar A11 basic) and combusted at 450°C for 5 hours (Heraeus chamber furnace, Heraeus Instruments GmbH, Germany). The weight was measured to the nearest 1 µg before and after the combustion. The same experiment was carried out with pieces of red coloured corals originated from the same location.

The amount of organic matter was calculated from the difference in the weight before and after the combustion.

## 2.6 Measurements

### 2.6.1 Measuring total alkalinity

Total alkalinity (TA) was analysed as described by Dickson *et al.* (eds. 2007, SOP 3b). This measuring technique is a potentiometric, open-cell titration using a 0.005 N hydrochloric acid for analysis. TA was measured by means of a semi automatic titration device (Metrohm Titrando 808, Deutsche Metrohm GmbH & Co. KG, Germany). The software package tiamo version 1.2 was used for the measurement.

The pH electrode of the device was calibrated every week with a three-point calibration in certified buffers (pH 4, 7, 9, Carl-Roth, Germany).

Prior to measurement, approximately 10 ml of sample were weighed reading to 0.0001 g (Sartorius balance RC 210D, accuracy: ± 0.001 g) to determine the exact volume and then 0.2 µm filtrated using syringe filter (Sarstedt, Filtropur S PAT, non-pyrogenic, sterile-R). Determination of TA was carried out at standard temperature of 20°C thus the acid was kept in a water bath for the term of analysis. The measuring mode was a monotonic equivalent-point titration (MET) which means the titrant was added using a constant (0.2 ml) increment every 30 s until pH reached about 2.87. According to Dickson *et al.* (eds. 2007, SOP 3b), a duplicate analysis was performed and measurement was repeated when the difference exceeded 5 µmol/ kg. Precision was within 2 µmol/ kg. Certified reference material for ocean carbonate measurements (Dickson Standard Batch 88 and Batch 83, University of California, Marine Physical Laboratory, Prof. A.G. Dickson) was used for corrections of accuracy of analysis.

TA was computed from the Gran function applied to titrant volume as well as electromotive force measurements with a non-linear curve fitting algorithm implemented in Matlab (The MathWorks Inc., Version 6.5). A prepared Excel file was used for corrections of possible device drift and deviations from the Dickson Standards.



### 2.6.2 pH measurement

The pH was determined as electromotive force (e.m.f.) values using the MEAS U function of the alkalinity device at 20°C. Before starting the main experiment a calibration curve was implemented at different temperatures with a newly opened Dickson Standard (Batch 88). The obtained values were plotted against calculated pH values of the standard at measured temperatures. These pH values of the standard were computed by means of the CO2SYS Excel Macro (Dr. D. Pierrot utilising the code developed by Lewis and Wallace, 1998) using TA, DIC, salinity and nutrient data of the Dickson Standard but also the measured temperature. Free scale was chosen as pH scale, the dissociation constants from Dickson were used for the  $\text{KHSO}_4$  source as well as the constants from Mehrbach *et al.* (1973) as refitted by Dickson and Millero (1987). Such calibration was repeated prior the control experiment using the same constants, pH scale and data processing.

All measurements were done as duplicates. The pH values were calculated from measured e.m.f. values by use of the calibration curve instead of using the method described by Dickson *et al.* (eds. 2007, SOP 6a) because at  $\text{pH} < 7.8$  high deviations between both methods were observed. Although the samples were kept in a water bath at constant temperature fluctuations of the sample temperature did not supply efficient data with Dickson's method. Since the measuring method (MEAS U) of the alkalinity device was aligned for 20°C the analysis of pH was carried out at that temperature and the obtained values were corrected to the storing temperature of 15°C through CO2SYS Excel Macro, subsequently.

### 2.6.3 Measuring dissolved inorganic carbon

Samples for dissolved organic carbon (DIC) determination were taken with a 50 ml syringe (Infuject, sterile-R) and subsequently filled into 4 ml brown glass vials (Carl-Roth, Germany) without any air bubbles and immediately closed with screw caps (without hole, Carl Roth, Germany) containing a PTFE septum (Carl-Roth, Germany). The vials were sealed with Parafilm (Paul Marienfeld GmbH & Co. KG, Germany) and stored at 4°C until analysis.

DIC was analysed according to Stoll *et al.* (2001) by means of a spectrophotometric continuous-flow analysis. The samples were measured at 20°C by means of an autoanalyzer (Quattro, Bran+Luebbe) with an attached sampler (XY-2 sampler, Bran+Luebbe).

The determination was carried out as duplicate analysis including measurements of drift values (artificial seawater with salinity of 35 and known DIC concentration), standards (with known DIC concentration, freshly made prior to measurement adapted to the DIC range of the samples) and certified reference material (Dickson Standard Batch 88, Batch 80 or Batch 83)

The obtained raw data were corrected against the standards and density to convert the values into  $\mu\text{mol}/\text{kg}$  followed by a drift and Dickson Standard correction.

### 2.7 Determination of aragonite saturation state

Total alkalinity and pH data were selected for the calculation of  $\Omega_{\text{Ar}}$  by means of CO2SYS Excel Macro (Dr. D. Pierrot utilising the code developed by Lewis and Wallace, 1998). Measured temperature and salinity were also used as input conditions whereas nutrients were neglected because of low values (see measured data in Appendix). Free scale was chosen as pH scale, the dissociation constants from Dickson were used for the  $\text{KHSO}_4$  source as well as the constants from Mehrbach *et al.* (1973) as refitted by Dickson and Millero (1987). The entire data set was corrected to storage temperature of  $15^\circ\text{C}$  (output conditions).

### 2.8 Examination of skeleton surface structure

After completion of the experiment scanning electron microscopy (SEM) images of coral fragments from the main experiment were taken by means of a CamScan-CS-44 at the Institute of Geosciences (University of Kiel).

### 2.9 Data processing

Using the statistic module of SigmaPlot 11.0 (Systat Software Inc.) all statistical analyses were performed. Measured data were conducted using different non-linear regression functions for the dissolution experiments. An unpaired t-test was applied to test the colour varieties of *L. pertusa* for significant differences in the ash-free dry weight (see statistic table in Appendix).

All  $\text{pCO}_2$  treatments of the main and control experiments were plotted using a sigmoidal regression function after Chapman (3 parameters) and Michaelis-Menten kinetics (ligand binding, one site saturation). The control of the main experiment containing ambient seawater was plotted against a hyperbolic decay regression function (2 parameters).

The sigmoidal regression function can be described by the following equation:

$$y = a(1 - e^{-bx})^c \quad (5)$$

The ligand binding, one site saturation regression function was used for plotting the data by means of enzyme kinetics and can be termed as:

$$y = \frac{B_{\max} \times x}{K_d + x} \quad (6)$$

where  $B_{\max}$  stands for the maximum reaction rate and  $K_d$  is the Michaelis constant which represents the substrate concentration but in this case it was the time value at which the reaction rate reached half of its maximum value.

The control of the main experiment was plotted using a hyperbolic decay regression equation (2 parameters):

$$y = \frac{a \times b}{(b + x)} \quad (7)$$

### 3. Results

#### 3.1 Preliminary tests

The test run I showed a rise in alkalinity. This test should point out the appropriate pCO<sub>2</sub> values for the main experiment. Instead of using a wide range of pCO<sub>2</sub> concentrations as in this test run fewer treatments but more replicates were chosen for the main experiment (data not shown).

In the test run II total alkalinity showed a high increase for both silicones with a rise of approximately 400 μmol/ kg for the transparent and about 430 μmol/ kg for the black, acid-free silicone (data not shown). The black silicone also showed a high increase in TA in the control. Similarly, the wax consisting of 80 % paraffin and 20 % stearin revealed a rise in alkalinity of about 300 μmol/ kg (data not shown). The pure paraffin showed no change after ten days and only a slight rise after 16 days but showed an increase of about 100 μmol/ kg after 44 days (data not shown).

In the test run III samples treated with both cycloheximide and chloramphenicol showed a slight rise in alkalinity but a significant drop in pH similar to the autoclaved samples treated with that fungicide and antibiotic (data not shown). The samples treated with HgCl<sub>2</sub> indicated a slight decline in TA and pH. But alkalinity remained constant after a re-measurement after 12 days and pH rose to its initial value (data not shown). Therefore, HgCl<sub>2</sub> was chosen as an appropriate pre-treatment prior the main experiment and was also employed for poisoning the coral fragments used in the main experiment to inhibit possible biological activity during the experiment.

Although the procedure of the test run IV (see chapter 2.3 Preliminary tests) led to constant pH values total alkalinity declined by approximately 400 μmol/ kg after 30 days (data not shown). Coral material used for the control experiment was rinsed several times thoroughly after bleaching and sterilizing and was stored seven days in natural seawater for equilibration to seawater conditions.

### 3.2 Main experiment

The  $\Omega_{Ar}$  was calculated as described in chapter 2.7 Determination of aragonite saturation state. Calculations of  $\Omega_{Ar}$  by means of DIC and TA data revealed higher fluctuations in the calculated seawater carbonate system parameters compared to TA and pH used for the same calculations. These fluctuations resulted in lower  $R^2$  values (data not shown). Therefore, DIC data were neglected for the determination of  $\Omega_{Ar}$ .

A non-linear regression function with a sigmoidal equation (after Chapman, 3 parameters) (see equation 5) was used to plot the saturation state against time. This regression function indicated the best fit to data according to the obtained  $R^2$  (Figure 3.1). However, this equation did not reflect real reaction kinetics. Hence, all treatments were plotted again using enzyme kinetic regression (Figure 3.2) (see equation 6). Michaelis-Menten kinetics (non-linear, ligand binding, one site saturation) was close to real reaction kinetics where  $B_{max}$  corresponds to  $\Omega_{Ar}$  and the substrate concentration corresponds to time. Similar to enzyme reaction kinetics showing saturation with rising substrate concentration, the obtained  $\Omega_{Ar}$  revealed a saturation curve with increasing time due to dissolution of coral material.

The critical saturation state was determined by means of the Michaelis-Menten regression equation, plotted in a combined graph for all treatments. The obtained  $\Omega_{Ar}$  were 1.077 for the 1200 ppm CO<sub>2</sub> treatment and showed values below 1 with 0.983 and 0.971 for the 1800 and the 2500 ppm CO<sub>2</sub> treatments, respectively (Figure 3.3).

The control of the ambient treatment showed a decreasing trend in  $\Omega_{Ar}$  from initial values of 1.805 to  $\Omega_{Ar} = 0.942$  at day 36 due to declining pH (Figure 3.4).

The blanks of the main experiment showed a rise in  $\Omega_{Ar}$ . The 1200 ppm CO<sub>2</sub> treatment blank started with a value of  $\Omega_{Ar} = 0.877$  and at the end of the experiment 1.383 was reached (Figure 3.5). The other two treatment blanks acted similar with starting values of 0.643 for 1800 and 0.465 for 2500 ppm CO<sub>2</sub> and end points of 1.171 and 0.947, respectively (Figure 3.5).

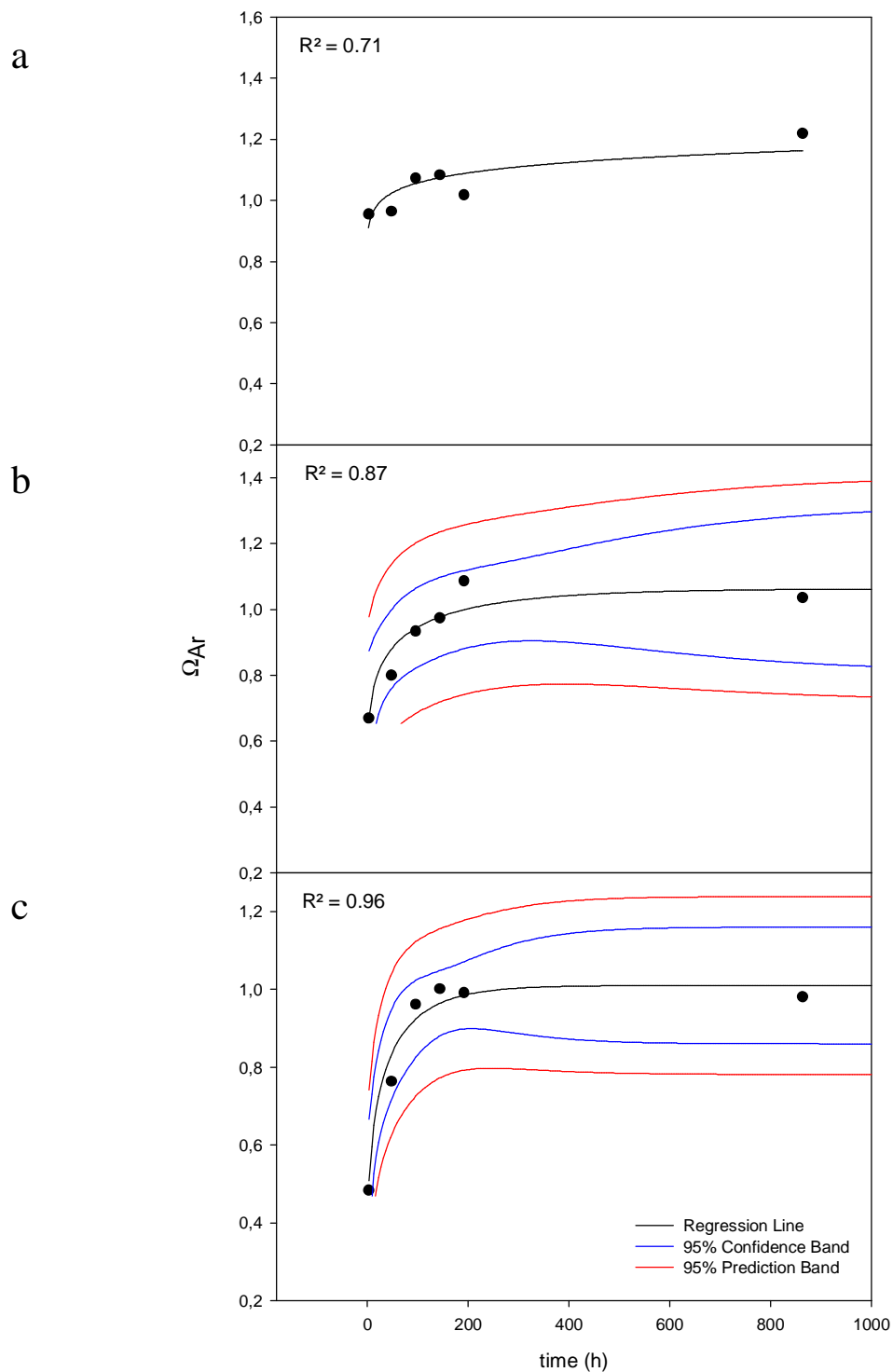


**Figure 3.1** Graphs a-c illustrating dissolution of the skeleton fragments with time by rising  $\Omega_{Ar}$  for all three treatments, 1200 (a), 1800 (b), and 2500 ppm CO<sub>2</sub> (c). The 95 % confidence and 95 % prediction bands are shown. Regression lines were plotted using non-linear regression with a sigmoidal equation after Chapman, 3 parameters.  $R^2$  values given in each graph.

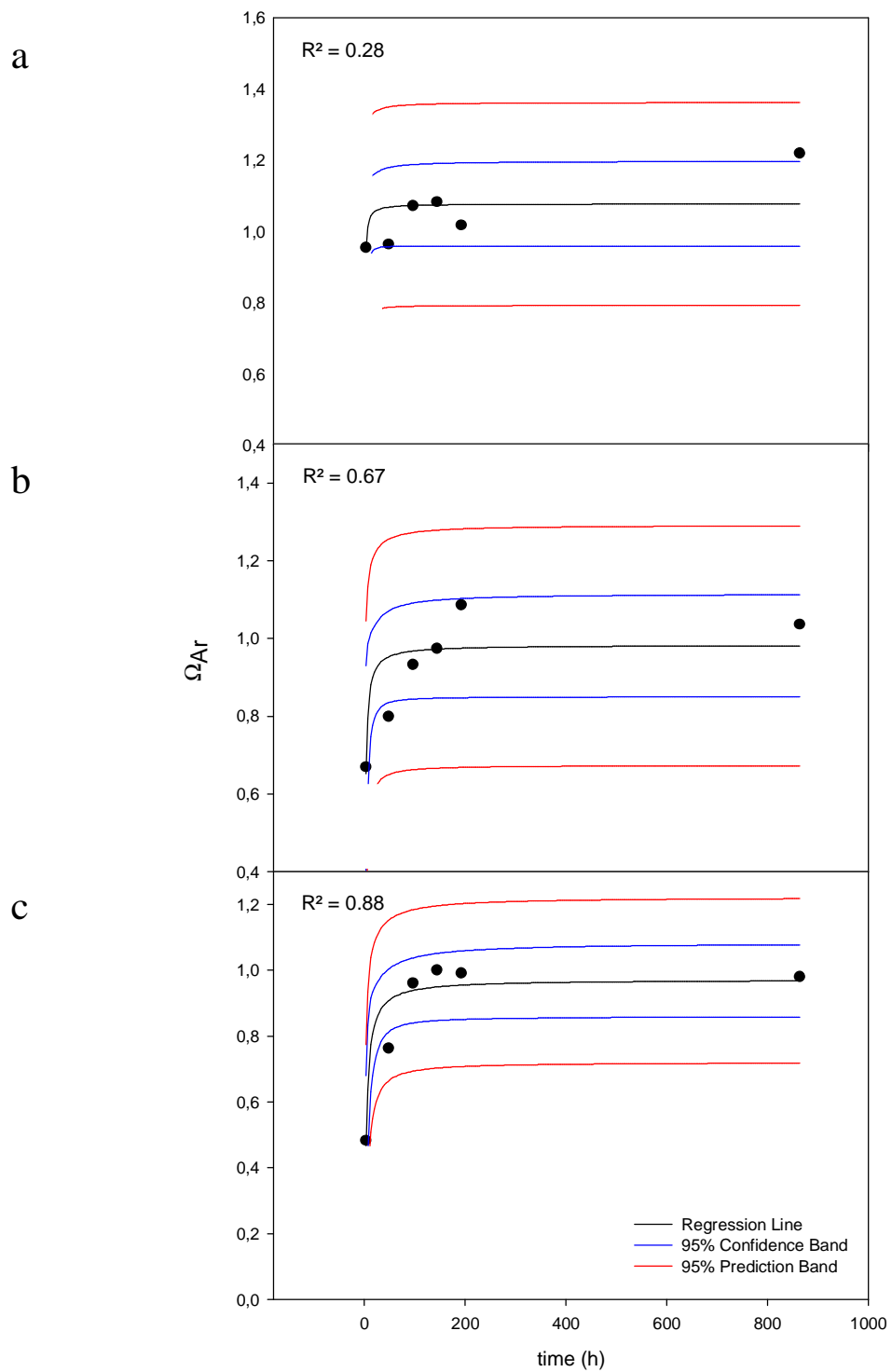


**Figure 3.2** Graphs a-c show increasing  $\Omega_{Ar}$  with time due to dissolution of coral skeleton fragments for the different treatments: 1200 (a), the 1800 (b), and 2500 ppm CO<sub>2</sub> (c). The 95 % confidence and 95 % prediction bands are given. Regression lines were plotted using non-linear regression, standard Michaelis-Menten kinetics, one site saturation. R<sup>2</sup> values given in each graph.

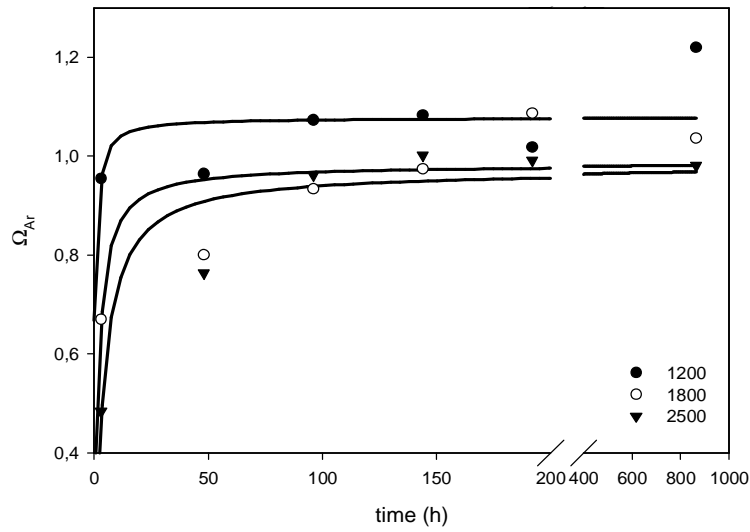


**Figure 3.3** Graph presents the development of  $\Omega_{Ar}$  for all three  $pCO_2$  treatments due to dissolution of the fragments. Regression lines were plotted using non-linear regression, standard Michaelis-Menten kinetics, one site saturation.

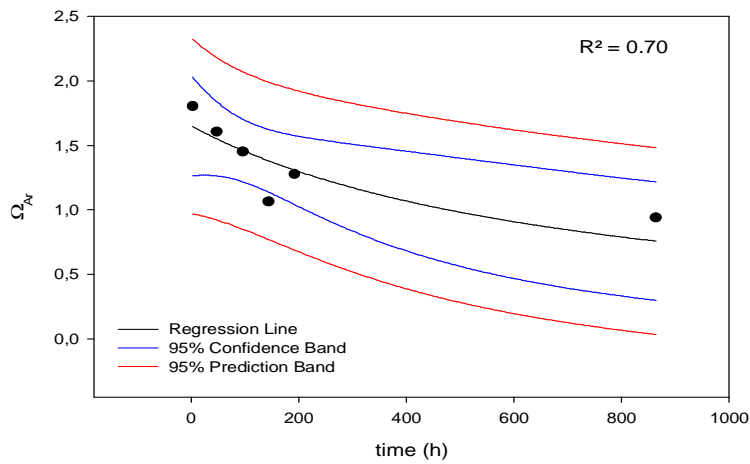


**Figure 3.4** Graph illustrating a decline in  $\Omega_{Ar}$  due to decreasing pH values for the control treatment using a hyperbolic decay regression, 2 parameters. The 95 % confidence and 95 % prediction bands are presented.  $R^2$  value given in graph.



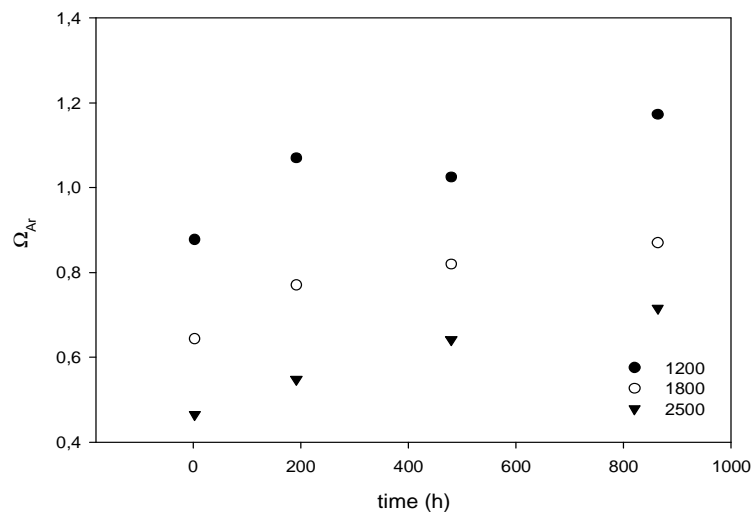


**Figure 3.5** Development of  $\Omega_{Ar}$  for the blanks of the different treatments due to outgasing via sampling.

### 3.3 Control experiment

The  $\Omega_{Ar}$  was calculated as described in chapter 2.7 Determination of aragonite saturation state. DIC data were neglected for the determination of  $\Omega_{Ar}$  (see explanation in previous chapter).

All wooden air stones used for the CO<sub>2</sub> bubbling were found to be overgrown by a biofilm. Additionally, one hosepipe connecting the air stone with the supply of CO<sub>2</sub>-enriched air contained visible algae contamination.

Although sigmoidal regression function (after Chapman, 3 parameters) showed the best data fit with very good R<sup>2</sup> (Figure 3.6) Michaelis-Menten kinetics accorded best with reaction kinetics (Figure 3.7). Standard Michaelis-Menten equation presented critical saturation values of  $\Omega_{Ar} = 1.257$  for S<sub>I</sub> and  $\Omega_{Ar} = 0.795$  for S<sub>II</sub> of the 2400 ppm CO<sub>2</sub> treatments (Figure 3.8). These obtained values resulted in a difference of 36.8 % between both experimental set-ups.

The controls containing ambient water showed different results in this experiment (data not shown). The control of S<sub>II</sub> revealed a decline in  $\Omega_{Ar}$ . In contrast, the control of S<sub>I</sub> remained relatively constant and fluctuated between  $1.71 \leq \Omega_{Ar} \leq 1.79$  (not shown).

The blanks of the bubbled 2400 ppm CO<sub>2</sub> treatment and the control blank of S<sub>I</sub> with ambient seawater showed relatively constant values, the latter fluctuated between

$1.83 \leq \Omega_{Ar} \leq 1.94$  (not shown). The blank of the 2400 ppm CO<sub>2</sub> treatment of S<sub>1</sub> revealed a slight rise due to outgasing of CO<sub>2</sub> via sampling (Figure 3.9).

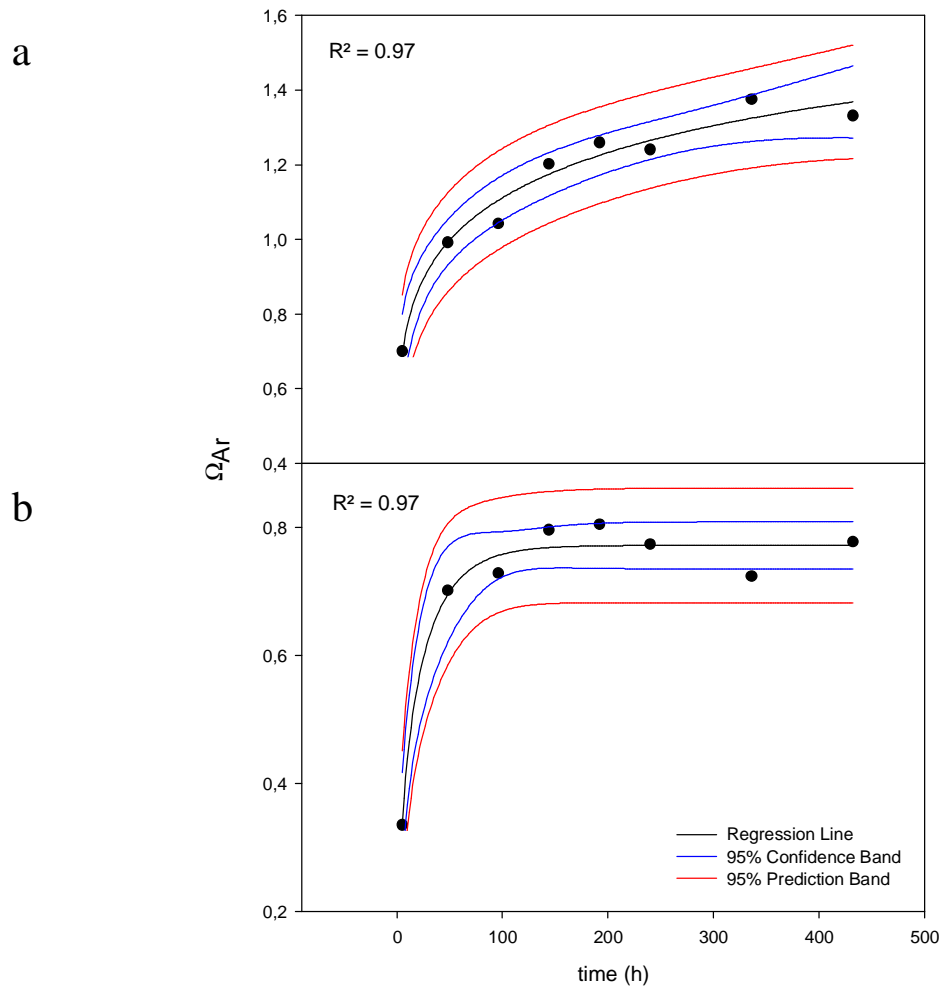


**Figure 3.6** Graphs a, b showing the development of  $\Omega_{Ar}$  due to dissolution of coral fragments for the different experimental set-ups: the 2400 ppm CO<sub>2</sub> treatments of sub-experiment one (a) and sub-experiment two (b). Each graph presents the 95 % confidence and 95 % prediction bands. Regression lines were plotted using non-linear regression with a sigmoidal equation after Chapman, 3 parameters.  $R^2$  values given in each graph.

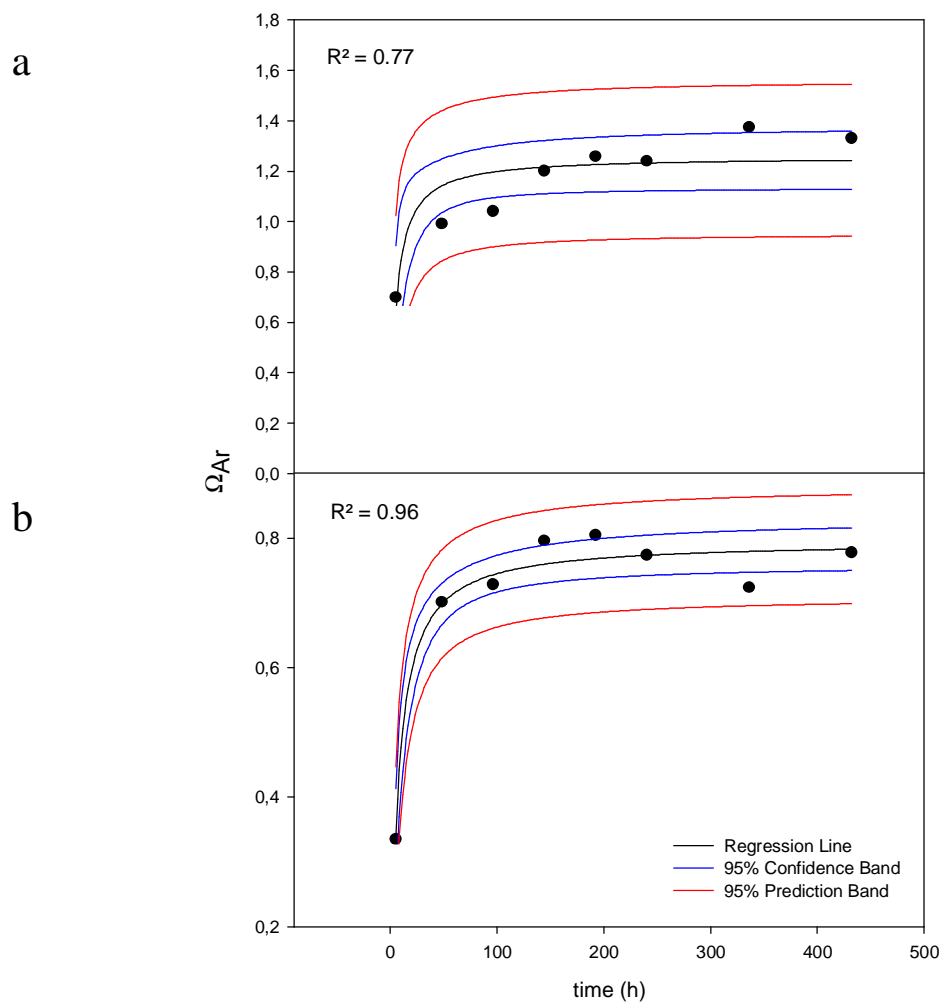


**Figure 3.7** Graphs a, b showing increase in  $\Omega_{Ar}$  for  $S_I$  (a) and  $S_{II}$  (b) caused by dissolving of coral material. Regression lines were plotted using non-linear regression, standard Michaelis-Menten kinetics, one site saturation.  $R^2$  values given in each graph.

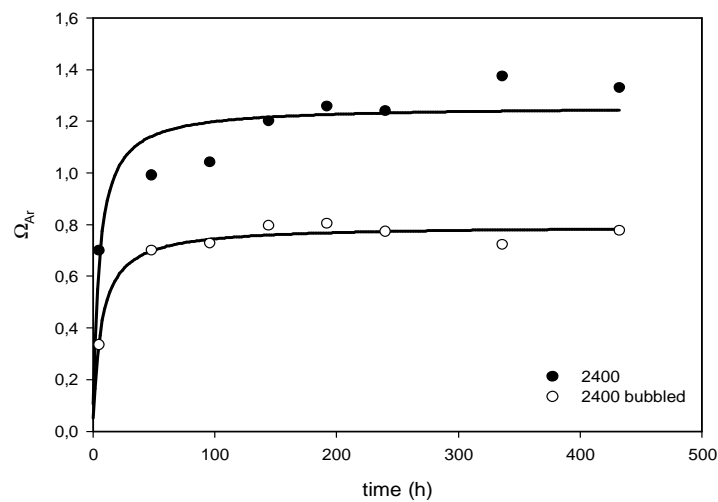


**Figure 3.8** Graph for control experiment illustrating dissolution of coral skeletons by increasing  $\Omega_{Ar}$  with time for the different set-ups. Regression lines were plotted using non-linear regression, ligand binding, one site saturation.

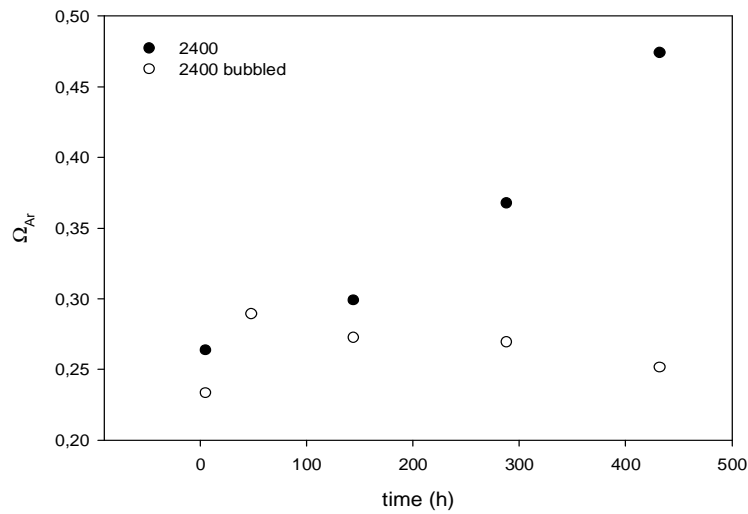


**Figure 3.9** Blanks for the control experiment presenting the development of  $\Omega_{Ar}$  for the 2400 ppm  $CO_2$  set-ups by bubbling with  $CO_2$ -enriched air or manipulation of the water, respectively. The blank of  $S_I$  showed an increase in due to outgasing via sampling whereas the blank of  $S_{II}$  showed relatively constant values.

#### 3.4 Determination of organic content in skeleton

The content of the organic compounds within skeleton was determined for white and red colour varieties of *Lophelia pertusa* by means of ash-free dry mass (AFDM). The white type showed a weight loss of  $3.37 \pm 0.22$  % and the red type exhibited a slightly lower value with  $3.11 \pm 0.27$  % (Table 3.1). Statistical analysis (t-test) indicated a significant difference in the ash-free dry weight between both colour varieties ( $P = 0.001$ ) (see statistical data in Appendix). Table 3.1 presents the differences in weight after combustion as well as the percentage weight loss for both colour varieties.

**Table 3.1** Ash-free dry weight and percentage weight loss of white and red types of *L. pertusa*. The determination of the dry weight failed for polyp number one for the red type due to loss of material.

White colour variety			Red colour variety		
Polyp number	AFDM (mg)	Weight loss (%)	Polyp number	AFDM (mg)	Weight loss (%)
1	12.205	3.232	1	-	-
2	14.316	3.773	2	14.201	2.873
3	11.927	3.362	3	14.085	2.860
4	11.396	3.082	4	14.152	2.876
5	12.580	3.311	5	16.873	3.416
6	12.547	3.317	6	15.875	3.219
7	13.343	3.519	7	16.647	3.393
<b>Mean</b>		<b>3.371</b>	<b>Mean</b>		<b>3.106</b>
<b>Std. deviation</b>		<b>0.221</b>	<b>Std. deviation</b>		<b>0.268</b>

Skeleton densities of *Lophelia pertusa* were measured ranging from 2.746 to 2.780 g/ cm<sup>3</sup> with a mean density of  $2.772 \pm 0.011$  g/ cm<sup>3</sup> (Form in preparation).

### 3.5 Examination of skeleton surface structure

To investigate visible dissolution effects on the skeleton surface, the outer wall of calices and septa were analysed and compared. Both coral parts presented “bumps” spread over the entire surface. These “bumps” seemed to have a smoother appearance and were commonly bigger on the outer wall whereas on septa, they were smaller and partly revealed mineral crystals on the summit. Furthermore, these structures revealed “corrosion spots” which were interpreted as dissolution impacts.

The ambient treatment showed healthy looking “bumps” which were intact both, on the outer wall and on septa (Figure 3.10).

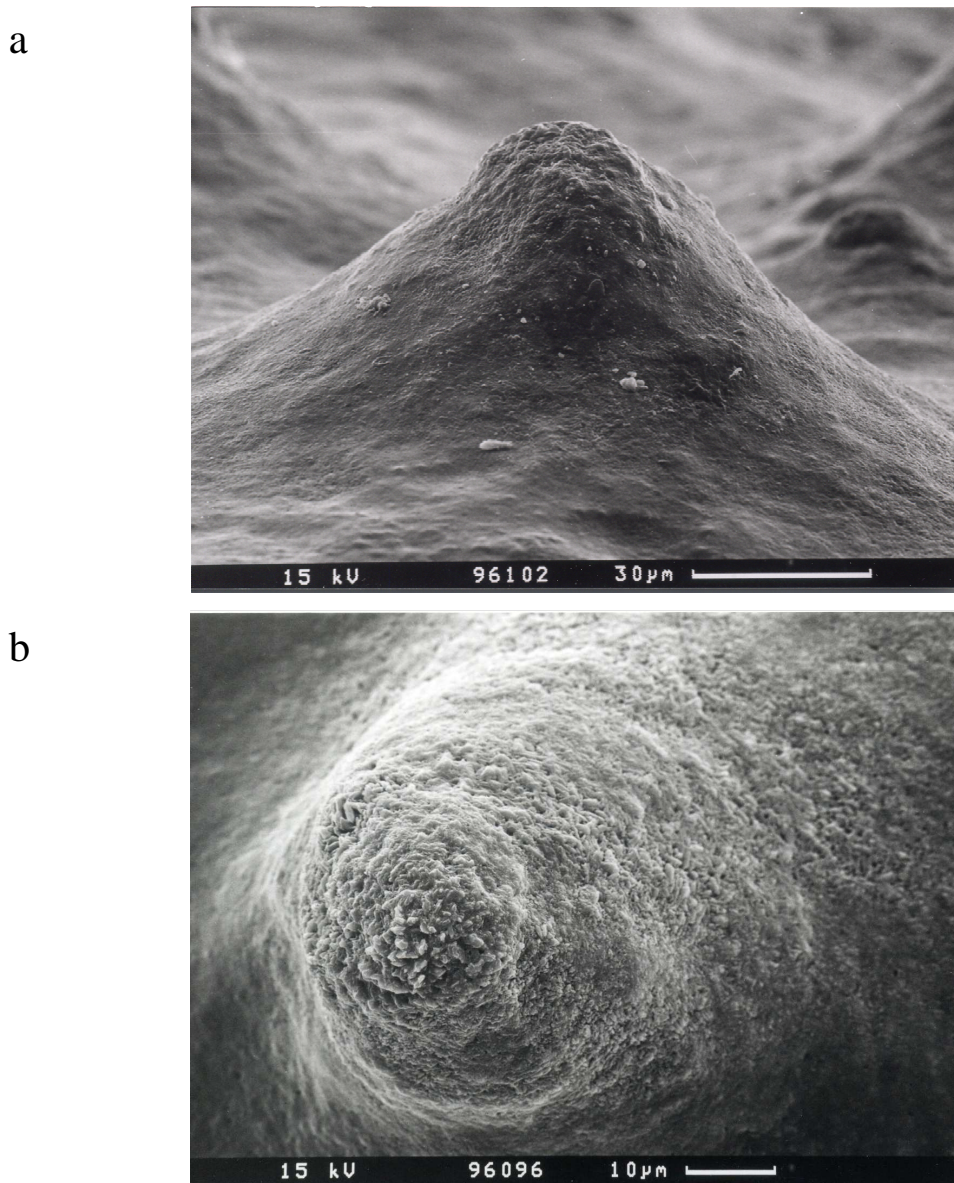


**Figure 3.10** SEM images of fragment samples of the control showing “bumps” on outer calyx wall (a) and on septa (b). Magnification was 910 x (a) and 1370 x (b). Scale: 30 µm for a and 10 µm for b.

The surface structures on skeletons of the 1200 ppm CO<sub>2</sub> treatment also seemed unscathed to the greatest extent. However, some subtle “corrosion spots” were found (Figure 3.11). Particles visible on the surface of the skeleton could be salt crystals, paraffin particles left from sealing or dust particles (Figure 3.11 a)

Figure 3.11 also gave a good comparison of the morphological differences in these “bumps” between outer wall and interior like the septa. “Bumps” on the outside of skeleton seemed to have a smooth summit (Figure 3.11 a) whereas single aragonite crystals could be recognised on the summit on septa “bumps” (Figure 3.11 b) as mentioned before.

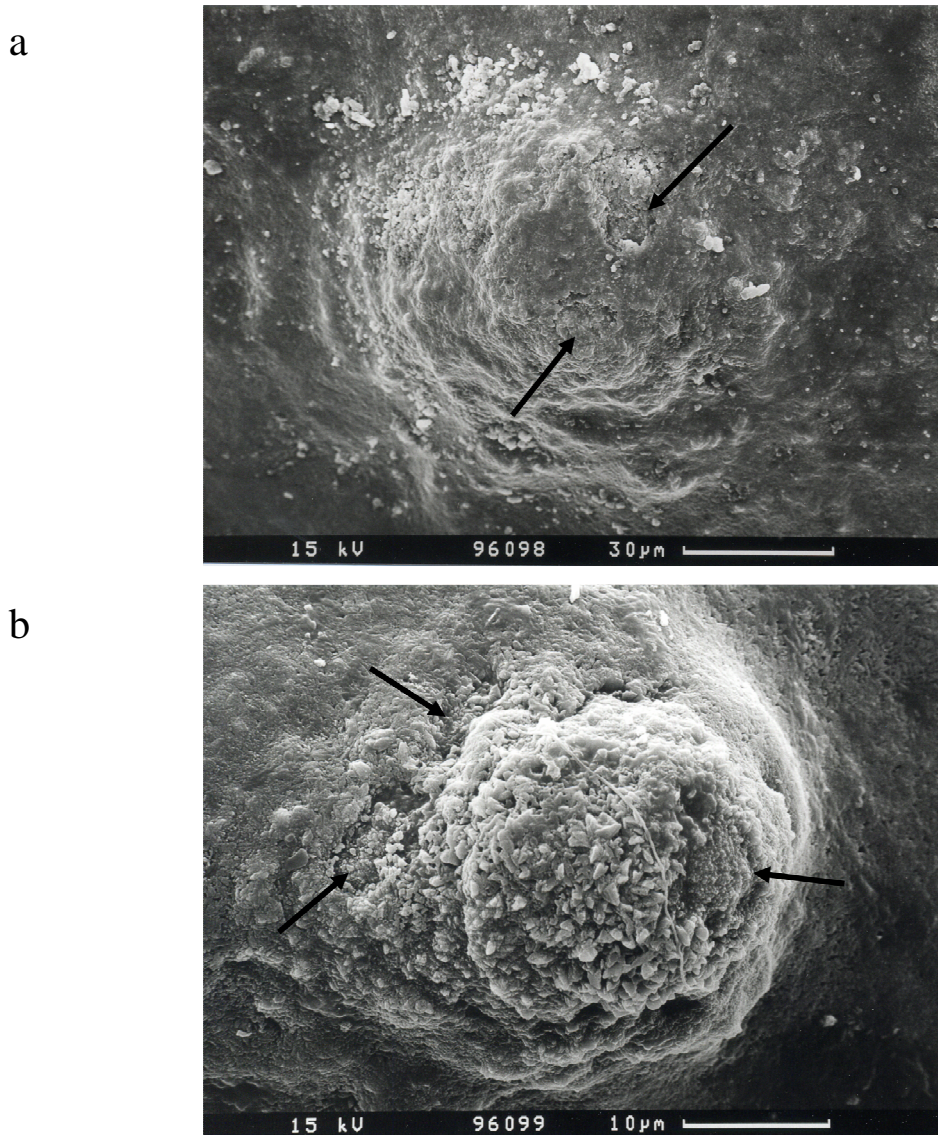
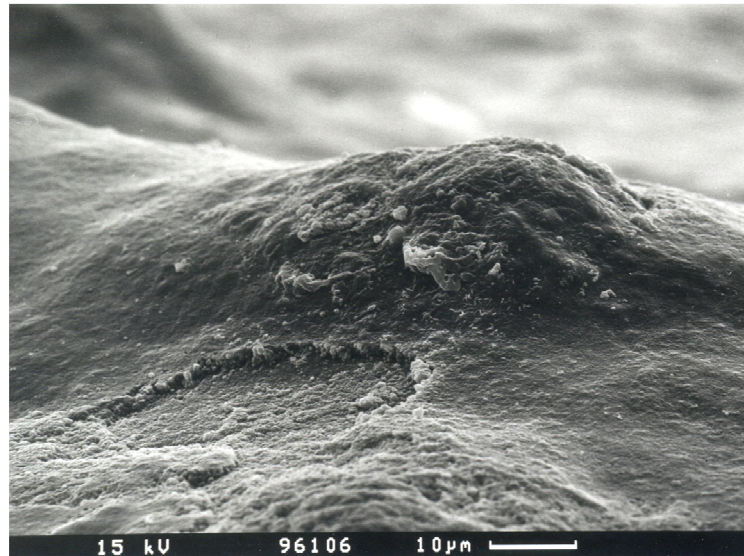


**Figure 3.11** SEM images of coral fragments from the 1200 ppm CO<sub>2</sub> treatment exhibiting subtle dissolution spots (arrowed) on the outer wall of the calyx (a) and on septa (b). Images were magnified 800 x (a) and 2310 x (b). Surface of skeleton showed many particles (a) (see explanation in text). Scale: 30 μm for a and 10 μm for b.

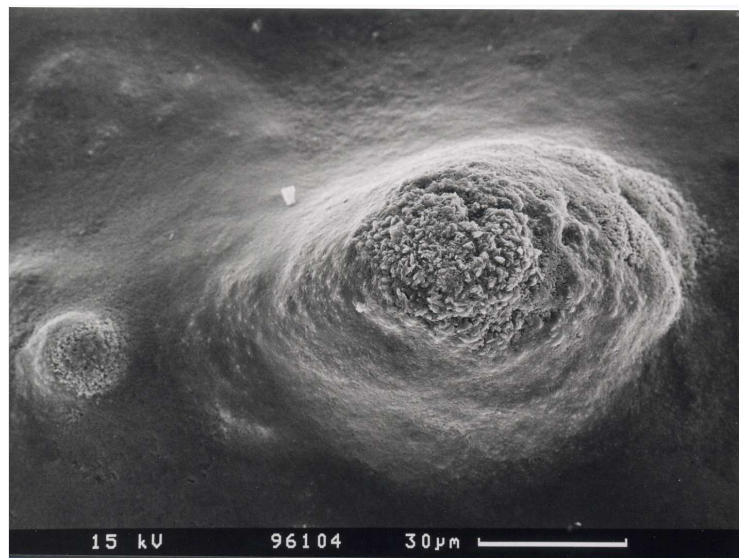
The surface of fragments exposed to 1800 ppm CO<sub>2</sub> showed bigger and deeper dissolution spots even next to “bumps” on the outer wall of calyx (Figure 3.12 a). However, “bumps” on septa were intact showing no evidence of dissolution (Figure 3.12 b); one single damaged “bump” was found (Figure 3.12 c).

The brighter particles on the right lower slope of the “bump” in Figure 3.12 c were possibly paraffin remains. But particles closely below the summit seemed to detach from the crest itself.

a



b



c

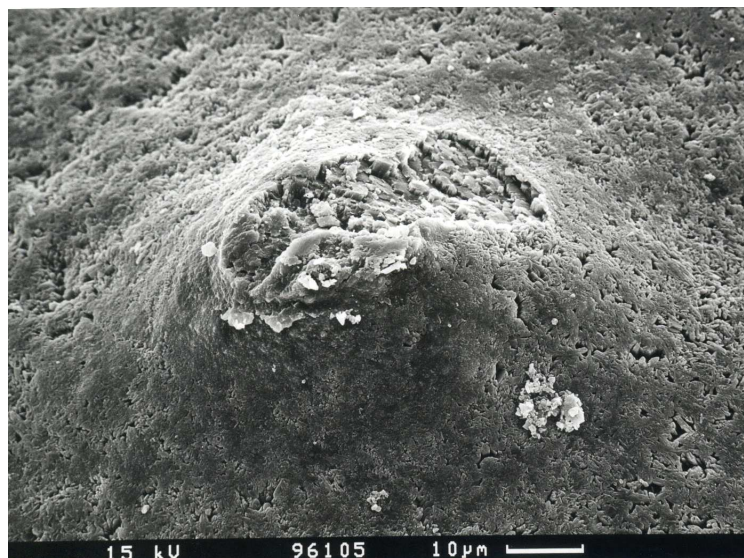


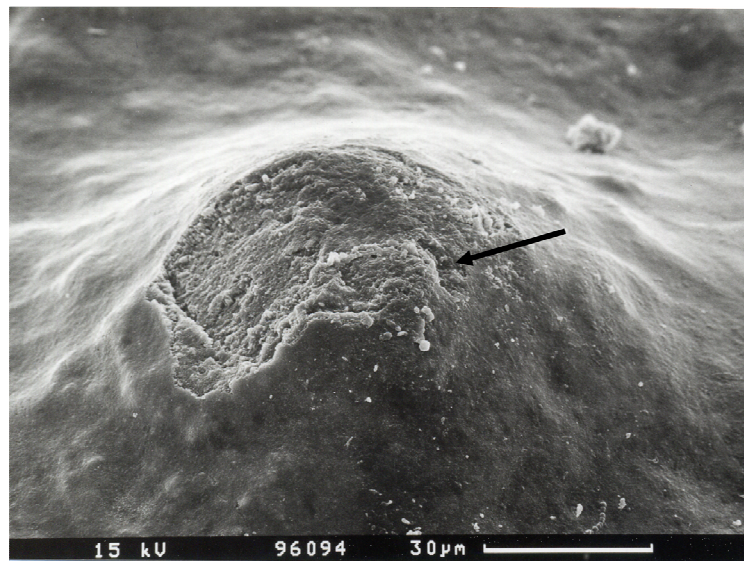
**Figure 3.12** SEM images of coral samples of the 1800 ppm CO<sub>2</sub> treatment revealing “corrosion spots” on the outside of skeleton (a) as well as on septa (c). Most “bumps” on the septa showed no visible effects of dissolution (b). Magnification was 1380 x (a), 800 x (b) and 1200 x (c). Scale: 10 μm for a, c and 30 μm for b.



Most “bumps” of the highest (2500 ppm CO<sub>2</sub>) treatment were affected by dissolution and partly showed severe damage both, on the outer wall of calices (Figure 3.13 a) and on septa (Figure 3.13 b) but also intact “bumps” were found.

The left part of the upper summit in Figure 3.13 a seemed to be scraped away probable mechanically but the centre of the upper slope was assumed to be affected by dissolution (arrowed). The deep “corrosion spot” in Figure 3.13 b exhibited fine aragonite needles. The particle on the right lower slope could be a drop of the glue used for the preparation of the SEM plates or a dust particle (Figure 3.13 b).

a



b

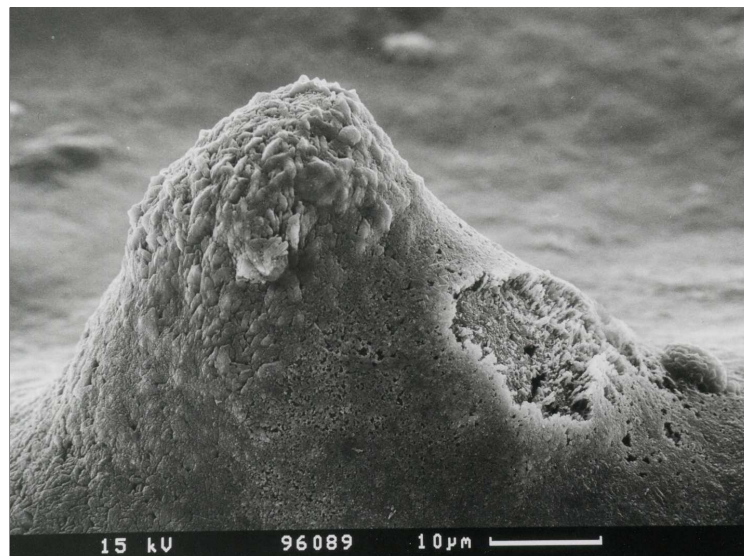


**Figure 3.13** SEM images of coral fragments from the 2500 ppm pCO<sub>2</sub> treatment showing dissolution spots on the outer calyx wall (a) (arrowed) as well as deep ones on septa (b) revealing aragonite needles. Images were magnified 1000 x (a) and 1800 x (b). Scale: 30 μm for a and 10 μm for b.

The detail (Figure 3.14 b) of Figure 3.14 a also showed parts of septa which were most likely scraped off mechanically but also revealed dissolution effects to lesser extent (arrowed).

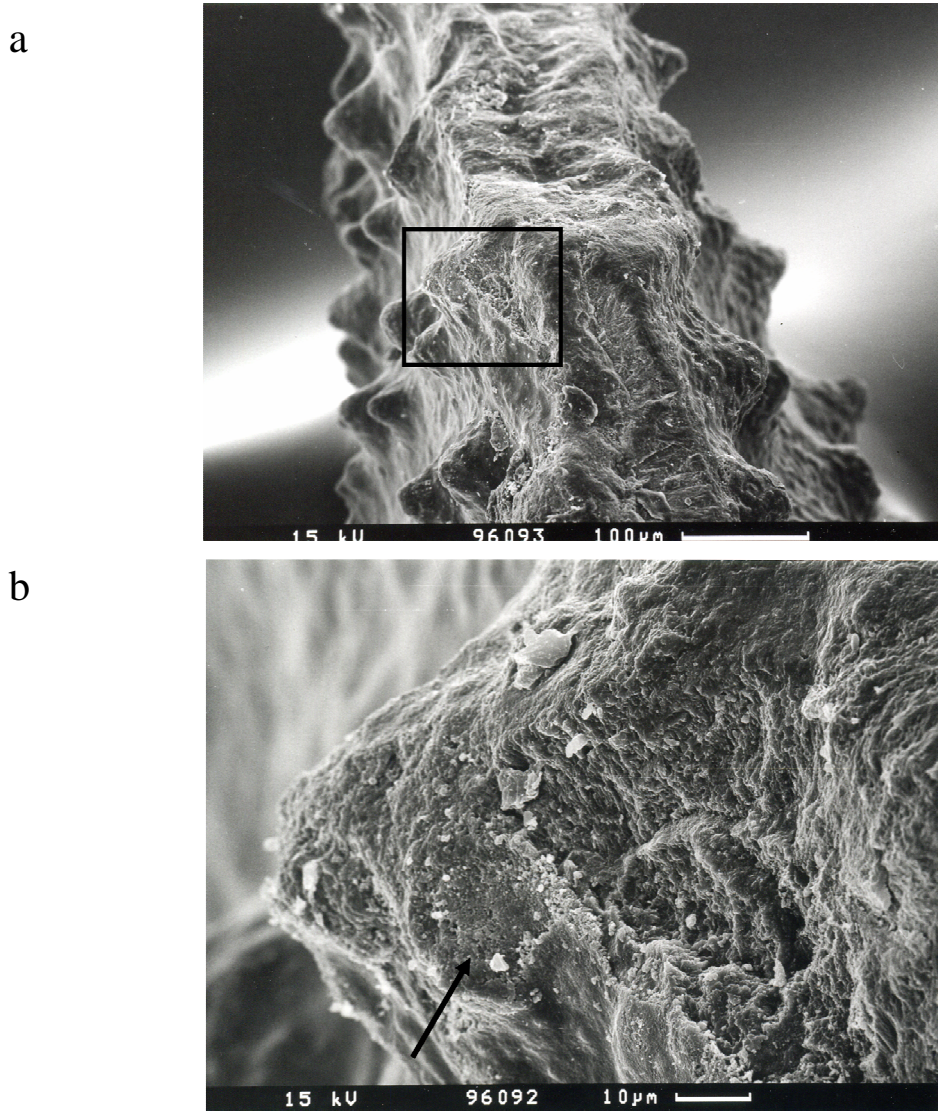
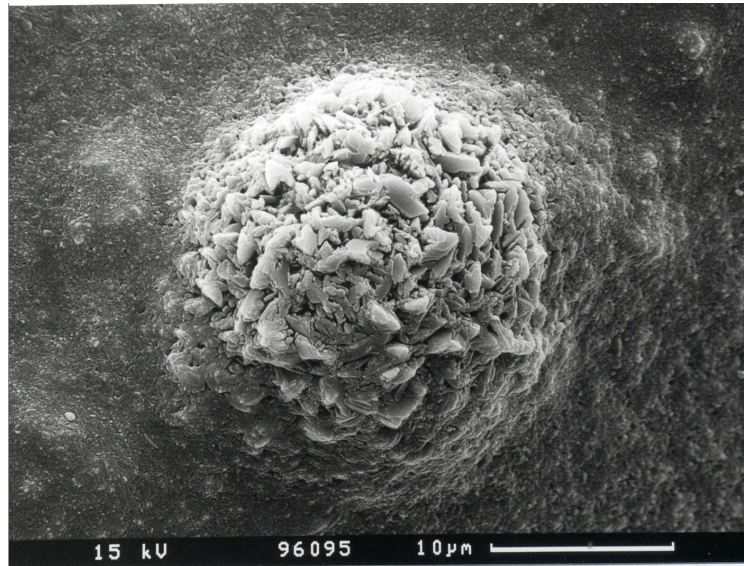


**Figure 3.14** SEM images of a coral fragment from the 2500 ppm CO<sub>2</sub> treatment exhibiting mechanical damage and dissolution spots on septa. Detail of a presenting scraped part on the right side and a slight spot of dissolution (arrowed) (b). Magnification was 200 x (a) and 1200 x (b). Scale: 100 µm for a and 10 µm for b.

Crystals of coral fragments of the control treatment revealed a rosette-like orientation concerning the lancet-shaped crystal tips (Figure 3.15 a). Most visible crystals of samples of the highest pCO<sub>2</sub> treatment showed no recognisable difference to that of the control samples but some crystals appeared to be rounded off (Figure 3.15 b arrowed).

a



b



**Figure 3.15** SEM images showing crystal morphology of a non-acidified coral sample of the control (a) and a fragment of the 2500 ppm CO<sub>2</sub> treatment (b) both on septa. Image a presented healthy looking crystals whereas in the centre left of image b rounded crystals were visible (arrowed). Magnification was 2800 x (a) and 3000 x (b). Scale: 10 μm for a and 3 μm for b.

## 4. Discussion

### 4.1 Precision of measured data

In total, 825 TA measurements were conducted including duplicate determinations of the samples and the certified reference material for accuracy of analysis. This amount of measurements was divided into 150 samples from all preliminary tests, 85 samples from the main experiment and 46 from the control experiment.

Concerning pH measurements, a difference in measured 0.1 mV corresponded to a change of 0.002 pH units.

Statistical analysis was employed to calculate the mean standard deviation and the mean coefficient of variance for the main and the control experiment by use of statistic functions of Excel (Microsoft Office Excel 2003, Microsoft Corporation) (Table 4.1).

**Table 4.1** Mean standard deviation and coefficient of variance for both experiments.

	Main Experiment		Control Experiment	
	Mean standard deviation	Mean coefficient of variance (%)	Mean standard deviation	Mean coefficient of variance (%)
TA	1.61	0.07	1.61	0.07
pH	0.0053	0.0695	0.0024	0.0318
$\Omega_{Ar}$	0.012	1.153	0.005	0.518

The quality of the measured parameters was guaranteed by performing duplicate analysis and measurements of certified reference material which resulted in low mean standard deviation and coefficient of variance, thus revealing the high precision of analysis.

### 4.2 Main experiment

The main experiment was carried out to find the critical aragonite saturation state under which skeletons of *Lophelia pertusa* start to dissolve.

To evaluate the results,  $R^2$  was used as quality criterion for the regression graphs. Although the sigmoidal regression function after Chapman presented the best fit to data (Figure 3.1), this regression did not show real reaction kinetics. Therefore, only the enzyme regression plots (Figures 3.2 and 3.3) were discussed in further detail.

To enhance the statistical power of the analysis,  $R^2 < 0.80$  were not considered. Consequently, the 1200 ppm  $\text{CO}_2$  treatment ( $R^2 = 0.28$ ) was excluded from further

consideration. The other two CO<sub>2</sub> treatments (1800 and 2500 ppm CO<sub>2</sub>) revealed higher R<sup>2</sup>, especially the highest treatment.

The entire experiment originally comprised a time period of 50 days. However, values between days eight and 36 were excluded because of large fluctuations in the measured carbonate system parameters (see below). At day 36 the seventh bottle of each treatment and the fifth of the control, respectively, were sampled which were unopened beforehand and thus showed no outgasing via growing headspace. Therefore, the obtained saturation states of the last day were regarded to be equilibrated with the acidified water. Sampling day 50 was also excluded because it was a re-measurement of the bottle opened at day 36.

The observed fluctuations between start and end values of the experiment were most likely caused by decreasing pH. According to dissolution kinetics and carbonate chemistry the pH should have risen as total alkalinity. However, the 1200 ppm CO<sub>2</sub> treatment showed an initial increase in pH from 7.672 to 7.719 followed by a drop to 7.499 and then rose again. The other treatments varied in a similar way. Therefore, only initial data and end values (not affected from fluctuations in the water chemistry, discussed below) were considered because high fluctuations in pH might superimpose effects of dissolution leading to variations in  $\Omega_{Ar}$  and could have affected precision of the critical  $\Omega_{Ar}$ .

These variations might have different reasons such as changes in water chemistry caused by paraffin used for sealing breaking edges and fissures of coral fragments. In the test run the first ten days showed no change concerning total alkalinity and pH, therefore paraffin was assumed to be the ideal sealing material. But it revealed a high increase in total alkalinity after 44 days (see chapter 3.1 Preliminary tests, test run II). Unfortunately, this test ran parallel with the main experiment after 7 days so it was not possible to separate effects caused by paraffin and dissolution in the main experiment. However, pH was less affected showing less pronounced fluctuations but coupled effects could be possible like interaction between skeleton and paraffin.

Furthermore, water chemistry might have been affected by bacterial respiration. To avoid disturbing micro-organisms the seawater used was 0.2  $\mu$ m filtered but coral fragments partly contained tissue remains which could not be removed without destroying the septa within the calices. Examinations of these remains of fragments from the main experiment exhibited an artificial bacterial fauna. The examination indicated airborne germs or

bacteria from water (Neulinger personal communication) which could have survived filtration or attached to corals during pre-treatments of skeleton material. Bacteria were determined by staining with DAPI which in turn gave no indication whether bacteria were alive or dead at period of observation. Moreover, the oxygen content of the water in the bottles was examined after completion of experiment showing 94 % oxygen saturation for the blank of the control and 83-84 % for treatment blanks which all contained no corals. However, decreased oxygen saturations of 72-73 % were measured for all treatments containing coral fragments strongly indicating the presence of micro-organisms. Despite poisoning with mercury chloride bacteria might have survived in microhabitats within calices (see details in chapter 1.5.2 Micro- and macrohabitats) containing air bubbles or in biofilms. Attached air bubbles and biofilms could have shielded bacteria from the toxin. Moreover, bacterial activity could also explain data progression of the control treatment (see Figure 3.4). Since  $\text{CO}_2$  is released by respiration, it could have acidified the water in the closed system resulting in declining pH. When saturation had fallen below its threshold, alkalinity rose due to dissolution. Although dissolution was observed in the ambient seawater treatment dissolving of  $\text{CaCO}_3$  could probably not compensate acidification caused by biological processes of bacteria.

Measurement of dissolved organic carbon (DOC) could have given an explanation about the portion of organic substances which serve as nutrition for bacteria and also include  $\text{H}_2\text{CO}_3$  and  $\text{CO}_2$  which in turn could change water chemistry according to carbonate buffer reactions (see equation 2 and explanations in chapter 1.7 Climate change and ocean acidification as well as references therein). Unfortunately, the DOC measuring system at the IFM-GEOMAR was not operating and thus analysing of DOC was not possible.

Moreover, effects caused by skeleton composition could also possibly change pH and therefore  $\Omega_{\text{Ar}}$ . When the saturation state reaches values near equilibrium, dissolution becomes surface-controlled (see explanation in chapter 1.9 Dissolution kinetics) (Morse and Arvidson 2002b) which implies that the organic matrix and its associated crystals control further dissolution. Therefore, highly corrosive water could dissolve coral fragments as far as the organic matrix because most susceptible parts vanish first under severe undersaturation (Berger 1967). The so exposed organic fraction could react with the undersaturated water which in turn could influence pH and water chemistry.

In conclusion, reasons for the observed fluctuations were not possible to be identified within the scope of this work. But it is certain that many different parameters influence dissolution and may thus change reaction kinetics.

#### 4.3 Control experiment

This experiment was performed to evaluate the obtained  $\Omega_{Ar}$  of the main experiment by applying different methods and pre-treatment of samples, respectively.

As in the main experiment, enzyme kinetics (ligand binding, one site saturation) (see Figures 3.7 and 3.8) revealed reaction kinetics close to the real ones and thus were considered in more detail. Again, the obtained  $R^2$  values served as quality criterion. The regression equation of this experiment exhibited relative high  $R^2$  values for both treatments with 0.77 for the non-bubbled ( $S_I$ ) and 0.96 for the bubbled ( $S_{II}$ ) 2400 ppm  $CO_2$  treatment indicating good conformity with enzyme kinetics and thus true reaction kinetics.

Possible effects of algal contamination of wooden air stones used in the bubbled experimental set-up could not be verified by the results.

Differences between both regression curves of this experiment could be the consequence of the different methods applied. In sub-experiment one, growing headspace due to outgasing via sampling resulted in higher saturation states compared to sub-experiment two (see Figure 3.7 and 3.8) in which  $pCO_2$  values remained constant over the entire sample period apart from fluctuations caused by constant perturbation from the gas mixing device.

Differences to the 2500 ppm  $CO_2$  treatment of the main experiment concerning  $\Omega_{Ar}$  could be explained by pre-treatment of samples. Coral material without paraffin sealing was crushed to rubble prior experiment to create more reactive surface area which was assumed to result in faster and more pronounced dissolution (Morse *et al.* 1979). Furthermore, the material was bleached and sterilized to eliminate any disturbing micro-organisms and tissue remains.

According to Berger (1967) and Honjo and Erez (1979), bleaching of biogenic carbonates enhances dissolution but their findings cannot be confirmed in this study. Nevertheless, the 2400 ppm  $CO_2$  treatment of  $S_{II}$  exhibited high initial alkalinities of  $> 3000 \mu mol/ kg$ . Notwithstanding, impacts of sterilizing may superimpose bleaching effects.

Sterilizing resulted in a drop of TA, especially in S<sub>I</sub>, which in turn led to different aragonite saturation states than in the main experiment. The lower  $\Omega_{Ar}$  value obtained from the 2400 ppm CO<sub>2</sub> treatment compared to that of the 2500 ppm CO<sub>2</sub> treatment of the main experiment was probably caused by bubbling itself implying constant water chemistry conditions related to the saturation state. Since bleaching and sterilizing resulted both in removal or destruction of disturbing organic material the S<sub>I</sub> control exhibited constant values fluctuating between  $1.71 \leq \Omega_{Ar} \leq 1.79$  but the S<sub>II</sub> control showed decreasing  $\Omega_{Ar}$  due to the decline in TA.

The reason for this decline in TA is unknown but it could be possible that sterilizing breaks bonds between structural elements and leads to the loss of functional groups which are then reconnected with ions from surrounding water, or sterilization may change crystal structure or mineral texture (Gaffey *et al.* 1991). In summary, it can be stated that sterilizing effects and dissolution might influence one another resulting in decreasing alkalinity and thus in a different  $\Omega_{Ar}$  than in the main experiment.

#### 4.4 Summary of main and control experiment

Treatments revealing good R<sup>2</sup> as quality criterion (R<sup>2</sup> > 0.8) exhibited an  $\Omega_{Ar} < 1$  concerning enzyme kinetics (Figure 4.1). The 2500 ppm CO<sub>2</sub> treatment of the main experiment seems to be the most trusted value of this study because the bubbled 2400 ppm CO<sub>2</sub> treatment of the control experiment has shown a very low critical saturation state due to the decline in TA (see previous chapter). On the other hand, relating the findings of this work to environmental conditions in the field it appears likely that the  $\Omega_{Ar}$  obtained by the CO<sub>2</sub>-bubbling experiment (S<sub>II</sub>) is probably closer to the real critical aragonite saturation state than that obtained from the 2500 ppm CO<sub>2</sub> treatment since currents at reef sites continuously supply corals with corrosive water. However, possible changes caused by sterilization and bleaching should be taken into consideration. Thus, it is suggested that the real critical  $\Omega_{Ar}$  for *Lophelia pertusa* is between 0.795 and 0.971.

Furthermore, it has to be emphasized that both  $\Omega_{Ar}$  values have been obtained by applying different methods. The  $\Omega_{Ar}$ , presented here, also depends on the constants and pH scale chosen for calculation implying that different constants and pH scales reveal a distinct  $\Omega_{Ar}$ .



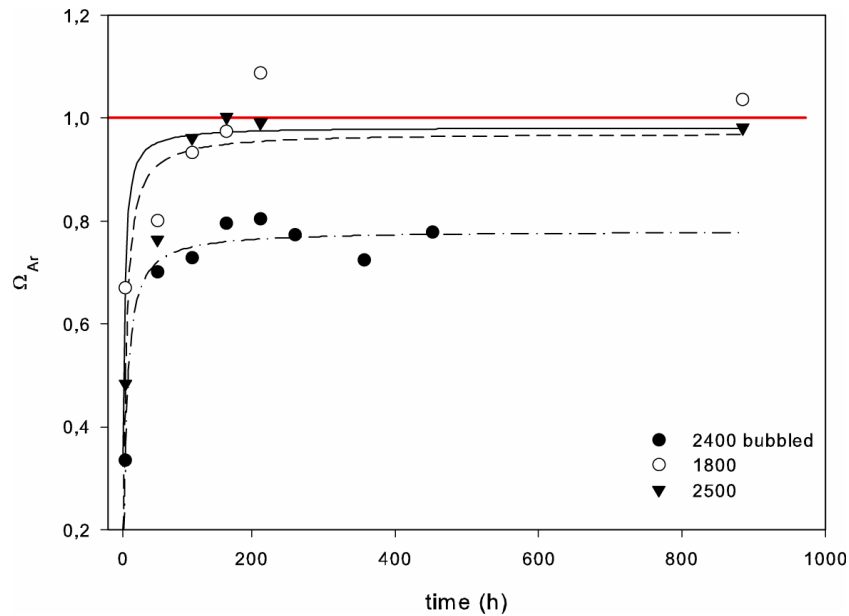


**Figure 4.1** Graph showing increase in  $\Omega_{Ar}$  with time due to dissolution of coral fragments from the main and control experiment revealing a critical  $\Omega_{Ar} < 1$ . The threshold value of  $\Omega_{Ar} = 1$  is presented in the graph (red line). Regression lines were plotted using non-linear regression, standard Michaelis-Menten kinetics, one site saturation. Regression lines shown for treatments exposed to 1800 (solid line) and 2500 ppm CO<sub>2</sub> (dashed line) from the main experiment and for the bubbled 2400 ppm CO<sub>2</sub> treatment (dash-dotted line) from the control experiment.

#### 4.5 Determination of organic content in coral skeleton

Determination of the ash-free dry weight (AFDM) presented a simple method to determine organic portions within coral skeletons.

The content of organic compounds within skeletons of different coral species was examined by Cuif *et al.* (2004a). Although their findings referred mainly to the tropic zooxanthellate *Favia stelligera*, *Lophelia pertusa* was also examined in their study showing similar results to *F. stelligera*. The measured percentage weight loss of coral skeletons comprised both, organic compounds and water. They suggested that the lost water could be part of the organic matrix. Thus, the determined weight loss includes the organic compounds and water that could be bound loosely to the organic matrix or produced by thermal decomposition of this matrix (Cuif *et al.* 2004a, Gaffey *et al.* 1991). The entire fraction of organic matter was estimated to be about 2.5-3 % of total skeleton weight with species-specific variations (Cuif *et al.* 2004a,). However, this organic portion might be underestimated since not all organic compounds were destroyed when corals were heated to 800°C (Dauphin *et al.* 2006). In this study, the determination of the AFDM for both colour varieties of *Lophelia pertusa* revealed relatively high percentages of

organic content within the skeleton showing 3.37 % and 3.11 % of total weight with a range of 3.08-3.77 % and 2.86-3.42 % for the white and red type, respectively. The difference between the organic portions obtained by Cuif *et al.* (2004a) and in this work could arise from different methods applied. But the higher values of percentage weight loss, obtained here, were not the consequence of thermal degradation of aragonite since the fragments were combusted at temperatures below the thermal degradation value of aragonite which is 550°C according to Cuif *et al.* (2004a). Differences in the organic content could also result from investigating samples of distinct reef sites since it was indicated that skeleton densities were location-specific (CSA International, Inc. 2007) concerning deviations in density due to skeleton composition (see following chapter). Since the origin of the samples of *L. pertusa* used in the study of Cuif *et al.* (2004a) was not specified the organic content presented in their study gave no indication of location-specific differences. Furthermore, it has to be highlighted that white coloured fragments of different locations were used in this work (see locations in chapter 2.2.3 Coral material). But the relatively high variability of the organic portion obtained for both colour varieties suggests possible variations in skeletal composition within a single species at different locations. Moreover, the determination of the AFDM of white and red coloured fragments of *L. pertusa* indicated a significant difference between both colour varieties (t-test,  $P = 0.001$ ) suggesting a distinct skeleton composition for both types.

#### 4.6 Comparison between coral and abiogenic aragonite density

It is evident that the density of biogenic carbonates is distinct in different species since the content of associated elements (Cohen *et al.* 2006, Gaffey *et al.* 1991, Meibom *et al.* 2007, Zhong and Mucci 1989) and the composition of organic matrix (Cuif *et al.* 2004a, Cuif and Dauphin 2005b, Gaffey *et al.* 1991) varies between species. But there might also be variations within single species at different locations as mentioned above (CSA International, Inc. 2007, Dodds 2007). The determined density of *Lophelia pertusa* is clearly different from abiogenic aragonite being 2.772 g/ cm<sup>3</sup> for *L. pertusa* (Form in preparation) and 2.93 g/ cm<sup>3</sup> for pure aragonite (Weast and Astle 1980). Since the density depends on the composition of the skeleton this difference of about 5 % between both, *L. pertusa* and pure aragonite, could apparently account from the organic content within the skeleton. To some extent, these deviations could also be caused by crystal morphology controlled by environmental conditions like pH (CSA International, Inc. 2007) or by

containing further elements like  $\text{Sr}^{2+}$  or  $\text{Mg}^{2+}$  (Cohen *et al.* 2006, Meibom *et al.* 2007, Zhong and Mucci 1989).

#### 4.7 Examination of skeleton surface structure

SEM images were taken from coral fragments from the main experiment exposed to 1200, 1800, and 2500 ppm  $\text{CO}_2$  for analysis of visible effects of dissolution.

Images taken revealed distinct effects in form of “corrosion spots” on surface structures on the outer wall of calices and septa (see chapter 3.6 Examination of skeleton surface structure). Such surface structures (“bumps”) constitute an extension of surface area exposed to dissolution as well as elevations from plain surface presenting more reactive area to corrosive water. Furthermore, the examination of coral fragments from the main experiment showed that a rise in  $\text{pCO}_2$  led to an increasing number of “bumps” affected by dissolution. But still intact “bumps” were found in each  $\text{pCO}_2$  treatment. The depth of these “corrosion spots”, however, gave no indication of dissolution magnitude. So it can be assumed that dissolution spots on “bumps” present quantitative impacts rather than qualitative ones.

Crystal outgrowth on the interior parts of skeleton like septa (see Figures 3.11 b and 3.15 a) could probably persist due to protection by tissue when the coral is still alive. In contrast, the “bumps” on the outer calyx wall may be affected by dissolution immediately after retreat of the coenosarc during coral growth or after death of the polyp both resulting in bare skeleton. Therefore, reaction with the surrounding water could lead to the smoother appearance of these outer “bumps”.

The crystals at the summit of the inner “bumps” seemed to be rounded off by dissolution. However, this effect was not prominent within the different  $\text{pCO}_2$  treatments and was only found in a single sample of the highest treatment.

According to Berger (1967) dissolution removes carbonates layer-by-layer thinning the material thus it is unclear if the observed “corrosion spots” are entirely caused by dissolution. Additionally, it has to be considered that “bumps” could be damaged by handling due to removal of epifauna and sealing. This mechanically caused damage, however, seems to be rather possible at the outer skeleton surface than at the interior or septa.

#### 4.8 Dissolution kinetics

Statistical analysis of the main and control experiment were conducted by standard Michaelis-Menten regression function due to the close resemblance with dissolution kinetics of biogenic carbonates. The progression of both, Michaelis-Menten and dissolution kinetics can be described by saturation curves. Reaction curves of biogenic carbonates show a fast and linear increase in dissolution when exposed to highly corrosive waters and reaches a plateau approaching  $\Omega_{Ar} \approx 1$  (see for example Figures 3.3 and 3.8) (Morse and Arvidson 2002b). Since the reaction takes time to reach that saturation point dissolution can be regarded to contain a certain time aspect. Considering the sharp initial increase in  $\Omega_{Ar}$  in highly undersaturated water dissolution rates might be overestimated in experiments with short sample periods whereas long-term experiments could point out possible acclimatisation to water conditions.

Moreover, the low aragonite saturation state obtained in this study indicates a different solubility product of calcium carbonate concerning biogenic aragonite (see equation 4) since the solubility product, and therefore  $\Omega_{Ar}$ , given in literature refers to the pure mineral aragonite. Hence, dissolution itself is not only controlled by reaction kinetics but depends also on thickness and texture of material, organic cover as well as crystal structure (Honjo and Erez 1979, Kleypas and Langdon 2006, Morse and Berner 1972, Walter and Morse 1985); consequently different responses are most likely with respect to dissolution (Ries *et al.* 2009).

#### 4.9 Conclusion

The  $\Omega_{Ar}$  differs with respect to crystal morphology (Kleypas and Langdon 2006), location (CSA International, Inc. 2007, Dodds 2007) as well as skeletal composition (organic matrix and addition of other elements) (for example Cuif and Dauphin 2005b, Meibom *et al.* 2007, Zhong and Mucci 1989) indicating a species-specific critical saturation state with certain variations due to local conditions.

The critical  $\Omega_{Ar}$  for *Lophelia pertusa* obtained in this study ranged between 0.795 and 0.971 depending on methods used and pre-treatment of samples.

The organic content within skeleton was found to be 3.37 % and 3.11 % of total weight for white and red colour varieties of *L. pertusa*, respectively. This relatively high organic content of skeleton resulted in a lower density of *L. pertusa*, being 2.772 g/ cm<sup>3</sup> (Form in

preparation) compared to pure aragonite. The organic compounds may also strengthen framework stability by reducing the critical dissolution threshold. This low critical saturation state and the ability of calcification below  $\Omega_{Ar} = 1$  (Cohen *et al.* 2009a, Form and Riebesell submitted, Maier *et al.* 2009) indicate that cold-water corals, or *Lophelia pertusa* in particular, may not be highly vulnerable to acidification effects as assumed before. Cold-water corals already experience low saturation states in their natural habitat because of higher solubility of carbonates and increased natural concentrations of CO<sub>2</sub> in greater depths due to remineralization of organic material. So they could be adapted to a low saturated environment. Therefore, the assumed resistance of cold-water corals concerning dissolution could result in significant implications for predicting models.

## 5. Significance of work

To the author's best knowledge, this is the first study demonstrating that coral aragonite is thermodynamically stable below the generally assumed threshold of  $\Omega_{Ar} = 1$ .

The obtained  $\Omega_{Ar}$  range may be representative for dead coral skeleton. Since the major part of coral reefs consists of dead framework (Freiwald *et al.* 2004, Rogers 1999) the obtained range of saturation state can be regarded as the critical range for the entire *L. pertusa* reef including the coral rubble zone (see details on different reef zones in chapter 1.5.2 Micro- and macrohabitats). This assumption may hold true since the living coral zone comprises the smallest part of a cold-water reef (Freiwald *et al.* 2004, Rogers 1999). Furthermore, the dead coral framework presents the highest species richness also implying the significance of the low saturation state for the reef as ecosystem.

Moreover, the obtained  $\Omega_{Ar}$  range might be one example for cold-water corals which could be considered in prediction models for impacts of climate change and ocean acidification on cold-water coral reefs. This  $\Omega_{Ar} < 1$  does not imply that *Lophelia pertusa* is generally less endangered since an increase in  $\text{CO}_2$  leads to a shoaling of the carbonate saturation horizon. But impacts of acidification on cold-water coral reefs might not occur as soon as predicted by Guinotte *et al.* (2006) and Turley *et al.* (2007). Furthermore, this lower threshold value reinforces that calcification below  $\Omega_{Ar} = 1$  is possible (Cohen *et al.* 2009a, Form and Riebesell submitted, Maier *et al.* 2009). Therefore, healthy or at least growing reef complexes will be maintained even at undersaturated water conditions.

## 6. Outlook

The organic compounds within the skeleton led to lower densities of *Lophelia pertusa* skeletons and also resulted in the lower aragonite saturation state obtained. Therefore, the role of the organic content should be investigated in more detail as well as its impact on the skeleton stability. Additionally, further work should determine the composition of the organic matrix including different methods like isotopic and elemental analysis.

Further work should exclude sealing due to possible interactions with skeletal surfaces. But also scraping off of epifauna should be avoided to maintain unharmed, natural surface structures, or different removal methods have to be searched to ensure intact skeletons, in this way surface structures like the “bumps” can be investigated in more detail.

Besides, the critical  $\Omega_{Ar}$  of the entire reef structure (living community as well as dead framework) has to be determined to obtain threshold values valid at the ecosystem level. Additionally, the saturation state of bioeroded framework should also be determined for comparisons with dead and living framework since biological processes including bioerosion could strongly influence dissolution and thus  $\Omega_{Ar}$  (for example Andersson *et al.* 2009, Caldeira 2007, Kleypas and Langdon 2006, Kleypas and Yates 2009). Investigations of surface structures like the “bumps” could also be used for comparison of dissolution behaviour between the different reef zones.

Furthermore, it could be necessary to investigate the critical saturation state of other cold-water coral species to calculate an  $\Omega_{Ar}$  for cold-water coral ecosystems since the saturation state is assumed to be species-specific with local variations. Therefore, several saturation states for corals should be taken into consideration for predicting models concerning different local water properties.

The critical aragonite saturation state of *Lophelia pertusa* could be of significance for model predictions concerning impacts of ocean acidification on cold-water reefs but has to be verified by further studies.

Assuming that cold-water corals might be more resistant to ocean acidification to some extent, increasing seawater temperatures and coupled effects with climate change threaten

the corals due to probable changes in the water masses (Kleypas *et al.* 2006, Raven *et al.* 2005). Thus, impacts of climate change and ocean acidification should be investigated on ecosystem level as well as monitoring the environmental parameters like nutrient supply or currents since they have profound impacts on cold-water corals.



## Acknowledgement

This thesis was carried out at the IFM-GEOMAR and I am very grateful to the staff and PhD students for provision of implements and helpful advice.

I would like to thank Kai Schulz for his advice in chemical issues especially at the beginning of this work. Special thanks go to Jana Meyer and Andrea Ludwig for expertly measuring my DIC samples. I am very grateful to Ute Schuldt for her help and advice in preparing the SEM plates and to Arno Lettmann for his skills at the scanning electron microscope. Furthermore, I would like to thank Sven Neulinger for his expertise on bacterial fauna associated with *L. pertusa*.

Special thanks go to Vera Thiel for all help and support and she also offered helpful discussion on aspects of the life as scientist. I am also very grateful to Scarlett Sett for checking my English spelling and expression and for all useful advice to improve the manuscript. Thanks are also due to Silvana Gagliardi for sharing her flat with me for the duration of this thesis.

Most of all, I would like to thank Armin Form without whose guidance I would not have been able to accomplish this thesis. I am very grateful for his supervision and unlimited help and advice. I would also like to thank him for his guidance through all obstacles that came up and I am sure he did not always have an easy time with me. Moreover, I would like to thank Armin for his encouragement especially at the final stages of this work.

I am very grateful to my family and friends for all their patience and understanding that I did not get in touch for a long time. Special thanks go to Janina and Claudia for their friendship and good times as well as for their encouragement and support especially during the harder times.

## References

- Allemand D, Ferrier-Pagès C, Furla P, Houlbrèque F, Puverel S, Reynaud S, Tambutté É, Tambutté S and Zoccola D (2004) Biomineralisation in reef-building corals: from molecular mechanisms to environmental control, *Comptes Rendus Palevol* 3: 453-467
- Andersson AJ, Kuffner IB, Mackenzie FT, Jokiel PL, Rodgers KS and Tan A (2009) Net loss of CaCO<sub>3</sub> from a subtropical calcifying community due to seawater acidification: mesocosm-scale experimental evidence, *Biogeosciences* 6: 1811-1823
- Andersson AJ, Mackenzie FT and Bates NR (2008) Life on the margin: implications of ocean acidification on Mg-calcite, high latitude and cold-water marine calcifiers, *Marine Ecology Progress Series* 373: 265-273
- Barnett TP, Pierce DW, AchutaRao KM, Gleckler PJ, Santer BD, Gregory JM and Washington WM (2005) Penetration of human-induced warming into the world's oceans, *Science* 309: 284-287
- Berger WH (1967) Foraminiferal ooze: solution at depths, *Science* 156: 383-385
- Berner RA and Wilde P (1972) Dissolution kinetics of calcium carbonate in sea water: I. Saturation state parameters for kinetic calculations, *American Journal of Science* 272: 826-839
- Berner RA, Berner EK and Keir RS (1976) Aragonite dissolution on the Bermuda pedestal: its depth and geochemical significance, *Earth and Planetary Science Letters* 30: 169-178
- Beuck L and Freiwald A (2005) Bioerosion pattern in a deep-water *Lophelia pertusa* (Scleractinia) thicket (Propeller Mound, Northern Porcupine Seabight), in: *Cold-water Corals and Ecosystems*, Freiwald A and Roberts JM (eds.) Berlin, Heidelberg: Springer-Verlag, pp. 915-936.
- Blamart D, Rollion-Bard C, Meibom A, Cuif J-P, Juillet-Leclerc A and Dauphin Y (2007) Correlation of boron isotopic composition with ultrastructure in the deep-sea coral *Lophelia pertusa*: implications for biomineralization and paleo-pH, *Geochemistry Geophysics Geosystems* 8 (12)
- Bromley RG (2005) Preliminary study of bioerosion in the deep-water coral *Lophelia*, Pleistocene, Rhodes, Greece, in: *Cold-water Corals and Ecosystems*, Freiwald A and Roberts JM (eds.) Berlin, Heidelberg: Springer-Verlag, pp. 895-914.
- Buddemeier RW and Smith SV (1999a) Coral adaptation and acclimatization: a most ingenious paradox, *American Zoologist* 39: 1-9
- Buddemeier RW, Kleypas JA and Aronson RB (2004) *Coral Reefs and Global Climate Change: Potential Contributions of Climate Change to Stresses on Coral Reef Ecosystems*, Pew Center on Global Climate Change.
- Caldeira K (2007) What corals are dying to tell us about CO<sub>2</sub> and ocean acidification, in: *Oceanography* 20 (2): 188-195, *Roger Revelle Commemorative Lecture*, Washington, DC, 05 July 2007.

- Caldeira K and Wickett ME (2003) Anthropogenic carbon and ocean pH, *Nature* 425: 365
- Cicerone R, Orr JC, Brewer P, Haugan P, Merlivat L, Ohsumi T, Pantoja S and Pörtner H-O (2004) The ocean in a high CO<sub>2</sub> world, *EOS, Transactions, American Geophysical Union* 85 (37):351–353
- Cohen AL and Holcomb M (2009b) Why corals care about ocean acidification: uncovering the mechanism, *Oceanography* 22 (4):118–127
- Cohen AL, Gaetani GA, Lundälv T, Corliss BH and George RY (2006) Compositional variability in a cold-water scleractinian, *Lophelia pertusa*: new insights into “vital effects”, *Geochemistry Geophysics Geosystems* 7 (12)
- Cohen AL, McCorkle DC, de Putron S, Gaetani GA and Rose KA (2009a) Morphological and compositional changes in the skeletons of new coral recruits reared in acidified seawater: insights into the biomineralization response to ocean acidification, *Geochemistry Geophysics Geosystems* 10 (7)
- CSA International, Inc. (2007) *Characterization of northern Gulf of Mexico deepwater hard bottom communities with emphasis on Lophelia coral*, US Department of the Interior, Minerals Management Service, Gulf of Mexico OCS Region, New Orleans, LA: OCS Study.
- Cuif J-P and Dauphin Y (2005b) The two-step mode of growth in the scleractinian coral skeletons from the micrometre to the overall scale, *Journal of Structural Biology* 150: 319-331
- Cuif J-P, Dauphin Y, Berthet P and Jegoudez J (2004a) Associated water and organic compounds in coral skeletons: quantitative thermogravimetry coupled to infrared absorption spectrometry, *Geochemistry Geophysics Geosystems* 5 (11)
- Dauphin Y, Cuif J-P and Williams CT (2008) Soluble organic matrices of aragonitic skeletons of Merulinidae (Cnidaria, Anthozoa), *Comparative Biochemistry and Physiology* 150B: 10-22
- Dauphin Y, Cuif J-P, Massard P (2006) Persistent organic components in heated coral aragonitic skeletons-implications for palaeoenvironmental reconstructions, *Chemical Geology* 231: 26-37
- Davies AJ, Wisshak M, Orr JC and Roberts JM (2008) Predicting suitable habitat for the cold-water coral *Lophelia pertusa* (Scleractinia), *Deep-Sea Research I* 55: 1048-1062
- de Haas H, Mienis F, Frank N, Richter TO, Steinacher R, de Stigter H, van der Land C and van Weering TCE (2009) Morphology and sedimentology of (clustered) cold-water coral mounds at the south Rockall Trough margins, NE Atlantic Ocean, *Facies* 55: 1–26
- Dickson AG, Sabine CL and Christian RJ (eds.) (2007) *Guide to best practices for ocean CO<sub>2</sub> measurements*, PICES, Special Publication 3.
- Dodds LA (2007) The ecophysiology of the cold-water coral *Lophelia pertusa* (Scleractinia), PhD Thesis, University of Aberdeen

- Dodds LA, Roberts JM, Taylor AC and Marubini F (2007) Metabolic tolerance of the cold-water coral *Lophelia pertusa* (Scleractinia) to temperature and dissolved oxygen change, *Journal of Experimental Marine Biology and Ecology* 349: 205-214
- Dullo W-C, Flögel S and Rüggeberg A (2008) Cold-water coral growth in relation to the hydrography of the Celtic and Nordic European continental margin, *Marine Ecology Progress Series* 371: 165–176
- Fabry VJ, McClintock JB, Mathis JT and Grebmeier JM (2009) Ocean acidification at high latitudes: the bellwether, *Oceanography* 22 (4):160-171
- Feely RA, Doney SC and Cooley SR (2009) Ocean acidification: present conditions and future changes in a high-CO<sub>2</sub> world, *Oceanography* 22 (4): 36–47
- Feely, RA, Sabine CL, Lee K, Berelson W, Kleypas JA, Fabry VJ and Millero FJ (2004) Impact of anthropogenic CO<sub>2</sub> on the CaCO<sub>3</sub> system in the oceans, *Science* 305:362–366
- Form AU (2010) Influence of anthropogenic climate change on the ecophysiology of the cold-water coral *Lophelia pertusa*, PhD Thesis, Christian-Albrechts University of Kiel, in preparation
- Form AU and Riebesell U (2010) Acclimation to ocean acidification during long-term CO<sub>2</sub> exposure in the cold-water coral *Lophelia pertusa*, *Global Change Biology*, submitted for publication
- Freiwald A, Fosså JH, Grehan A, Koslow T and Roberts JM (2004) *Cold-water Coral Reefs*, UNEP-WCMC, Cambridge, UK.
- Freiwald A, Henrich R and Pätzold J (1997a) Anatomy of a deep-water coral reef mound from Stjernsund, West Finnmark, Northern Norway, *SEPM Special Publication* 56: 141-161
- Furla P, Galgani I, Durand I and Allemand D (2000) Sources and mechanisms of inorganic carbon transport for coral calcification and photosynthesis, *Journal of Experimental Biology* 203: 3445-3457
- Gaffey SJ, Kolak JJ and Bronnimann CE (1991) Effects of drying, heating, annealing, and roasting on carbonate skeletal material, with geochemical and diagenetic implications, *Geochimica et Cosmochimica Acta* 55: 1627-1640
- Gattuso J-P, Gao K, Lee K, Rost B and Schulz KG (2010) Approaches and tools to manipulate the carbonate system, in: Riebesell U, Fabry VJ, Hansson L and Gattuso J-P (eds.) *Guide to best practices for ocean acidification research and data processing*, Luxembourg: Publication Office of the European Union, pp. 41-52.
- Guinotte JM, Orr JC, Cairns S, Freiwald A, Morgan L and George R (2006) Will human induced changes in seawater chemistry alter the distribution of deep-sea scleractinian corals? *Frontiers in Ecology and the Environment* 4 (3):141–146

Hoegh-Guldberg O, Mumby PJ, Hooten AJ, Steneck RS, Greenfield P, Gomez E, Harvell CD, Sale PF, Edwards AJ, Caldeira K, Knowlton N, Eakin CM, Iglesias-Prieto R, Muthiga N, Bradbury RH, Dubi A and Hatzioios ME (2007) Coral reefs under rapid climate change and ocean acidification, *Science* 318: 1737-1742

Honjo S and Erez J (1979) Dissolution rates of calcium carbonate in the deep ocean; an *in-situ* experiment in the North Atlantic Ocean, *Earth and Planetary Science Letters* 40: 287-300

Hughes TP (1987) Skeletal density and growth form of corals, *Marine Ecology Progress Series* 35: 259-266

IPCC (2007) *Climate Change 2007: The Physical Science Basis, Contribution of Working Group I to the Fourth Assessment Report, The Intergovernmental Panel on Climate Change (IPCC)*, Cambridge, UK and New York, USA: Cambridge University Press.

Keir RS (1979) The dissolution kinetics of biogenic calcium carbonates in seawater, *Geochimica et Cosmochimica Acta* 44: 241–252

Kleypas JA and Langdon C (2006) Coral reefs and changing seawater chemistry, in: *Coral Reefs and Climate Change: Science and Management*, Phinney JT, Skirving W, Kleypas JA and Hoegh-Guldberg O (eds.) Washington, DC: American Geophysical Union, pp. 73–110.

Kleypas JA and Yates KK (2009) Coral reefs and ocean acidification, *Oceanography* 22 (4): 108-117

Kleypas JA, Feely RA, Fabry VJ, Langdon C, Sabine CL and Robbins LL (2006) *Impacts of Ocean Acidification on Coral Reefs and Other Marine Calcifiers: A Guide for Future Research*, report of a workshop held 18–20 April 2005, St. Petersburg, FL, sponsored by NSF, NOAA and the US Geological Survey.

Maier C, Hegeman J, Weinbauer MG and Gattuso J-P (2009) Calcification of the cold-water coral *Lophelia pertusa* under ambient and reduced pH, *Biogeosciences* 6 (8): 1671–1680

Marubini F, Ferrier-Pagès C, Furla P and Allemand D (2008) Coral calcification responds to seawater acidification: a working hypothesis towards a physiological mechanism, *Coral Reefs* 27: 491-499

Maynard JA, Baird AH and Pratchett MS (2008d) Revisiting the Cassandra syndrome; the changing climate of coral reef research, *Coral Reefs* 27: 745-749

Meibom A, Mostefaoui S, Cuif J-P, Dauphin Y, Houlbrèque F, Dunbar R and Constantz B (2007) Biological forcing controls the chemistry of reef-building coral skeleton, *Geophysical Research Letters* 34

Milliman JD (1975) Dissolution of aragonite, Mg-calcite and calcite in the North Atlantic Ocean, *Geology* 3: 461-462

Morse JW and Arvidson RS (2002b) The dissolution kinetics of major sedimentary carbonate minerals, *Earth-Science Reviews* 58: 51-84

Morse JW and Berner RA (1972) Dissolution kinetics of calcium carbonate in sea water: II. A kinetic origin for the lysocline, *American Journal of Science* 272: 840–851

Morse JW, de Kanel J and Harris K (1979) Dissolution kinetics of calcium carbonate in seawater: VII. The dissolution kinetics of synthetic aragonite and pteropod tests, *American Journal of Science* 279: 488–502

Orr JC, Fabry VJ, Aumont O, Bopp L, Doney SC, Feely RA, Gnanadesikan A, Gruber N, Ishida A, Joos F, Key RM, Lindsay K, Maier-Reimer E, Matear R, Monfray P, Mouchet A, Najjar RG, Plattner G-K, Rodgers KB, Sabine CL, Sarmiento JL, Schlitzer R, Slater RD, Totterdell IJ, Weirig M-F, Yamanaka Y and Yool A (2005b) Anthropogenic ocean acidification over the twenty-first century and its impact on calcifying organisms, *Nature* 437:681–686

Peterson MNA (1966) Calcite: rates of dissolution in a vertical profile in the Central Pacific, *Science* 154: 1542–1544

Pörtner H-O (2008) Ecosystem effects of ocean acidification in times of ocean warming: a physiologist's view, *Marine Ecology Progress Series* 373: 203-217

Puverel S, Tambutté É, Pereira-Mouriès L, Zoccola D, Allemand D and Tambutté S (2005b) Soluble organic matrix of two Scleractinian corals: partial and comparative analysis, *Comparative Biochemistry and Physiology* 141B: 480-487

Raven J, Caldeira K, Elderfield H, Hoegh-Guldberg O, Liss P, Riebesell U, Shepherd J, Turley C, Watson A, Heap R, Banes R and Quinn R (2005) *Ocean acidification due to increasing atmospheric carbon dioxide*, Policy document 12/05, The Royal Society, Cardiff, UK: The Clyvedon Press Ltd.

Riebesell U (2004) Effects of CO<sub>2</sub> enrichment on marine phytoplankton, *Journal of Oceanography* 60: 719–729

Riebesell U, Körtzinger A and Oschlies A (2009) Sensitivities of marine carbon fluxes to ocean change, *Proceedings of the National Academy of Sciences of the United States of America* 106 (49): 20602-20609

Riebesell U, Schulz KG, Bellerby RGJ, Botros M, Fritsche P, Meyerhöfer M, Neill C, Nondal G, Oschlies A, Wohlers J and Zöllner E (2007) Enhanced biological carbon consumption in a high CO<sub>2</sub> ocean, *Nature* 450:545–548

Riebesell U, Zondervan I, Rost B, Portell PD, Zeebe RE and Morel FMM (2000) Reduced calcification of marine plankton in response to increased atmospheric CO<sub>2</sub>, *Nature* 407: 364-367

Ries JB, Cohen AL and McCorkle DC (2009) Marine calcifiers exhibit mixed responses to CO<sub>2</sub>-induced ocean acidification, *Geology* 37 (12):1131–1134

Roberts JM, Wheeler AJ and Freiwald A (2006) Reefs of the deep: the biology and geology of cold-water ecosystems, *Science* 312: 543-547

Roberts JM, Wheeler AJ, Freiwald A and Cairns S (2009) *Cold-Water Corals: The Biology, Geology of Deep-Sea Coral Habitats*, New York: Cambridge University Press.

Rogers AD (1999) The biology of *Lophelia pertusa* (Linnaeus 1758) and other deep-water reef-forming corals and impacts from human activities, *International Review of Hydrobiology* 84 (4): 315-406

Rogers AD (2004) The biology, ecology and vulnerability of deep-water coral reefs, PhD Thesis, British Antarctic Survey, Cambridge

Schubert R, Schellnhuber H-J, Buchmann N, Epiney A, Griebhammer R, Kulesa M, Messner D, Rahmstorf S and Schmid J (2006) *Die Zukunft der Meere—zu warm, zu hoch, zu sauer*, Sondergutachten des Wissenschaftlichen Beirats der Bundesregierung Globale Umweltveränderungen (WBGU), Berlin.

Schulz KG, Barcelos e Ramos J, Zeebe RE and Riebesell U (2009) CO<sub>2</sub> perturbation experiments: similarities and differences between dissolved inorganic carbon and total alkalinity manipulations, *Biogeosciences* 6 (10):2145-2153

Silverman J, Lazar B and Erez J (2007a) Effect of aragonite saturation, temperature, and nutrients on the community calcification rate of a coral reef, *Journal of Geophysical Research* 112

Stoll MHC, Bakker K, Nobbe GH and Haese RR (2001) Continuous-flow analysis of dissolved inorganic carbon content in seawater, *Analytical Chemistry* 73 (17):4111-4116

Turley CM (2008) Impacts of changing ocean chemistry in a high-CO<sub>2</sub> world, *Mineralogical Magazine* 72 (1): 359-362

Turley CM, Roberts JM and Guinotte JM (2007) Corals in deep-water: will the unseen hand of ocean acidification destroy cold-water ecosystems?, *Coral Reefs* 26: 445-448

Walter LM and Morse JW (1985) The dissolution kinetics of shallow marine carbonates in seawater: a laboratory study, *Geochimica et Cosmochimica Acta* 49: 1503–1513

Weast RC and Astle MJ (1980) *Handbook of Chemistry and Physics—A Ready-Reference Book of Chemical and Physical Data*, 60th edition, Boca Raton, Florida: CRC Press.

Wheeler AJ, Beyer A, Freiwald A, de Haas H, Huvenne VAI, Kozachenko M, Olu-Le Roy K and Opderbecke J (2007) Morphology and environment of cold-water coral carbonate mounds on the NW European margin, *International Journal of Earth Sciences* 96 (1): 37-56

Wootton JT, Pfister CA and Forester JD (2008) Dynamic patterns and ecological impacts of declining ocean pH in a high-resolution multi-year dataset, *Proceedings of the National Academy of Sciences of the United States of America* 105 (48): 18848-18853

Zeebe RE and Wolf-Gladrow DA (2001) *CO<sub>2</sub> in Seawater: Equilibrium, Kinetics, Isotopes*, Elsevier Oceanography Series 65, Amsterdam: Elsevier, pp. 27-52.

Zhong S, Mucci A (1989) Calcite and aragonite precipitation from seawater solutions of various salinities: precipitation rates and overgrowth compositions, *Chemical Geology* 78: 283-299



## Appendix

### Appendix 1 Nutrient data

**Table A.1** Nutrients. The content of total silicon in the seawater used was measured prior the main experiment and phosphate, ammonia, nitrate, and nitrite were measured before the control experiment started. Values shown are means of a duplicate analysis. Units given in  $\mu\text{mol/l}$ .

Total Si	$\text{PO}_4^{3-}$	$\text{NH}_4^+$	$\text{NO}_3^-$	$\text{NO}_2^-$
8.91	0.22	1.65	1.05	0.21

## Appendix 2 Details on acidification for the main experiment

**Table A.2** Amounts of HCl and Na<sub>2</sub>CO<sub>3</sub> added for manipulation of natural seawater used in the main experiment. The concentrations of HCl and Na<sub>2</sub>CO<sub>3</sub> were 3.571 mol/ l and 2.000 μmol/ l, respectively. Water was weight to the nearest 0.1 g (Sartorius CPA 34001S, accuracy: ± 0.1 g). Total alkalinity and pH of the natural seawater were measured prior acidification and were TA = 2329.8 μmol/ kg and pH = 8.0612.

pCO <sub>2</sub> (ppm)	Amount of water (kg)	Addition of HCl (ml)	Addition of Na <sub>2</sub> CO <sub>3</sub> solution (ml)
control (480 )	6.001	0.000	0.000
1200	9.742	0.728	0.650
1800	10.608	1.101	0.983
2500	10.262	1.317	1.176

Appendix 3 Carbonate system parameters of the main experiment

**Table A.3a** Measured and calculated carbonate system parameters of the different main experiment treatments. Values shown for  $\Omega_{Ar}$  were calculated by use of means of measured TA and pH (free scale) for a salinity of 33.6 and 15°C applying CO2SYS Excel Macro. Measured DIC values are also given.

time (d)	Control (480 ppm CO <sub>2</sub> )				1200 ppm CO <sub>2</sub>				1800 ppm CO <sub>2</sub>				2500 ppm CO <sub>2</sub>			
	TA ( $\mu\text{mol/kg}$ )	pH	$\Omega_{Ar}$	DIC ( $\mu\text{mol/kg}$ )	TA ( $\mu\text{mol/kg}$ )	pH	$\Omega_{Ar}$	DIC ( $\mu\text{mol/kg}$ )	TA ( $\mu\text{mol/kg}$ )	pH	$\Omega_{Ar}$	DIC ( $\mu\text{mol/kg}$ )	TA ( $\mu\text{mol/kg}$ )	pH	$\Omega_{Ar}$	DIC ( $\mu\text{mol/kg}$ )
0	2299,4	7,9814	1,805	2166,3	2323,1	7,6717	0,955	2300,7	2334,8	7,5066	0,670	2334,1	2342,9	7,3575	0,484	2377,8
2	2291,5	7,9263	1,608	2184,6	2351,0	7,6707	0,964	2317,8	2391,7	7,5766	0,800	2398,4	2443,1	7,5455	0,764	2435,2
4	2300,9	7,8746	1,452	2228,4	2360,2	7,7186	1,073	2319,8	2411,0	7,6438	0,934	2408,1	2466,0	7,6470	0,962	2454,6
6	2334,4	7,7209	1,066	2314,5	2389,8	7,7172	1,083	2381,6	2454,3	7,6554	0,975	2434,4	2520,8	7,6555	1,002	2503,5
8	2316,1	7,8095	1,276	2270,7	2423,2	7,6817	1,018	2387,4	2434,9	7,7099	1,087	2426,0	2558,1	7,6440	0,992	2553,6
10	2330,2	7,6949	1,007	2318,9	2416,4	7,6823	1,032	2378,8	2431,6	7,6285	0,911	2399,5	2628,5	7,5379	0,809	2598,5
12	2365,1	7,5755	0,789	2383,5	2518,8	7,6148	0,916	2505,0	2450,1	7,5582	0,788	2488,9	2671,6	7,5189	0,789	2674,3
16	2647,7	7,5235	0,789	2641,8	2572,7	7,5351	0,787	2578,4	2605,7	7,5559	0,834	2612,2	2731,3	7,5108	0,792	2698,8
20	2587,9	7,5270	0,777	2602,6	2461,1	7,7061	1,090	2427,8	2591,7	7,5524	0,823	2587,1	2715,7	7,5420	0,843	2680,5
24	2633,8	7,5536	0,839	2642,2	2852,7	7,4995	0,807	2884,3	2877,9	7,5424	0,895	2941,1	2916,0	7,5183	0,860	2970,5
28	2726,7	7,5793	0,919	2696,3	2850,0	7,5345	0,871	2862,0	2594,3	7,6192	0,953	2592,1	3005,1	7,5676	0,988	3025,9
32	3192,9	7,4429	0,798	3245,8	2596,9	7,6559	1,033	2563,6	2612,7	7,6369	0,997	2601,2	3147,1	7,5297	0,953	3094,9
36	2548,3	7,6220	0,942	2563,0	2414,0	7,7682	1,220	2377,4	2926,0	7,6020	1,037	2853,9	2956,2	7,5720	0,981	2877,8
50	2758,4	7,5994	0,971	2698,5	2448,1	7,7683	1,238	2404,3	3135,6	7,5033	0,895	3067,2	3128,8	7,5393	0,967	3080,8

**Table A.3b** Measured and calculated carbonate system parameters of the blanks of the different main experiment treatments. Values shown for  $\Omega_{Ar}$  were calculated by use of means of measured TA and pH (free scale) for a salinity of 33.6 and 15°C applying CO2SYS Excel Macro. Measured DIC values are also given.

time (d)	Control (480 ppm CO <sub>2</sub> )				1200 ppm CO <sub>2</sub>				1800 ppm CO <sub>2</sub>				2500 ppm CO <sub>2</sub>			
	TA ( $\mu\text{mol/kg}$ )	pH	$\Omega_{Ar}$	DIC ( $\mu\text{mol/kg}$ )	TA ( $\mu\text{mol/kg}$ )	pH	$\Omega_{Ar}$	DIC ( $\mu\text{mol/kg}$ )	TA ( $\mu\text{mol/kg}$ )	pH	$\Omega_{Ar}$	DIC ( $\mu\text{mol/kg}$ )	TA ( $\mu\text{mol/kg}$ )	pH	$\Omega_{Ar}$	DIC ( $\mu\text{mol/kg}$ )
0	2298,1	7,9826	1,808	2137,3	2312,2	7,6346	0,877	2298,8	2328,2	7,4896	0,644	2335,2	2311,0	7,3457	0,465	2365,0
8	2303,1	8,0915	2,248	2167,8	2314,1	7,7267	1,070	2295,4	2343,6	7,5687	0,771	2335,7	2329,8	7,4163	0,548	2334,2
20	2309,7	8,0377	2,029	2161,5	2314,5	7,7066	1,025	2283,7	2324,8	7,6008	0,820	2338,2	2313,6	7,4913	0,642	2354,9
36	2332,6	8,0389	2,054	2165,9	2316,9	7,7693	1,173	2280,2	2325,8	7,6280	0,870	2324,9	2317,7	7,5398	0,715	2336,9
50	2505,4	8,2538	3,330	2303,5	2335,2	7,8440	1,383	2280,9	2335,7	7,7647	1,171	2308,8	2318,9	7,6686	0,947	2320,6

Appendix 4 Statistical report for the main experiment

**Table A.4a** Non-linear regression applied for the different pCO<sub>2</sub> treatments using dynamic fitting. Sigmoidal regression function after Chapman, 2 parameter.

pCO <sub>2</sub> (ppm)	R <sup>2</sup>	Std. error of estimate	P	Power with $\alpha = 0.05$	DF	SS
1200	0.7063	0.0684	0.1591	0.5627	5	0.0479
1800	0.8725	0.0718	0.0455	0.8331	5	0.1214
2500	0.9588	0.0541	0.0084	0.9764	5	0.2132

P = probability, DF = degrees of freedom, SS = sum of squares

**Table A.4b** Non-linear regression applied for the control treatment using dynamic fitting. Hyperbolic regression function, 2 parameters.

pCO <sub>2</sub> (ppm)	R <sup>2</sup>	Std. error of estimate	P	Power with $\alpha = 0.05$	DF	SS
480	0.7881	0.1946	0.0975	0.6859	5	0.5360

P = probability, DF = degrees of freedom, SS = sum of squares

**Table A.4c** Non-linear regression applied for the different pCO<sub>2</sub> treatments using dynamic fitting. Regression function for Michaelis-Menten kinetics, ligand binding, one site saturation

pCO <sub>2</sub> (ppm)	R <sup>2</sup>	B <sub>max</sub>	Std. deviation of B <sub>max</sub>	95 % confidence interval	DF	SS
1200	0.2768	1.0774	0.0432	0.9575 to 1.197	4	0.0346
1800	0.6679	0.9827	0.0477	0.8503 to 1.115	4	0.0403
2500	0.8773	0.9714	0.0403	0.8596 to 1.083	4	0.2620

DF = degrees of freedom, SS = sum of squares, B<sub>max</sub> = maximum reaction rate but corresponds here to  $\Omega_{Ar}$

Appendix 5 Details on acidification for the control experiment

**Table A.5** Amounts of HCl and Na<sub>2</sub>CO<sub>3</sub> added for manipulation of natural seawater used in the control experiment. The concentrations of HCl and Na<sub>2</sub>CO<sub>3</sub> were 3.571 mol/ l and 1.421 μmol/ l, respectively. Water was weight reading to 0.1 g (Sartorius CPA 34001S, accuracy: ± 0.1 g). Measurements of TA and pH prior acidification showed 2321.7 μmol/ kg for TA and 8.1479 for pH.

pCO <sub>2</sub> (ppm)	Amount of water (kg)	Addition of HCl (ml)	Addition of Na <sub>2</sub> CO <sub>3</sub> solution (ml)
control (380 )	11.468	0.000	0.000
2400	11.454	1.685	2.118

Appendix 6 Carbonate system parameters of the control experiment

**Table A.6a** Measured and calculated carbonate system parameters of the control experiment treatments. Values shown for  $\Omega_{Ar}$  were calculated by use of means of measured TA and pH (free scale) for a salinity of 33.3 and 15°C applying CO2SYS Excel Macro. Measured DIC values are also given.

time (d)	non-bubbled								bubbled							
	Control (380 ppm CO <sub>2</sub> )				2400 ppm CO <sub>2</sub>				Control (400 ppm CO <sub>2</sub> )				2400 ppm CO <sub>2</sub>			
	TA ( $\mu\text{mol/kg}$ )	pH	$\Omega_{Ar}$	DIC ( $\mu\text{mol/kg}$ )	TA ( $\mu\text{mol/kg}$ )	pH	$\Omega_{Ar}$	DIC ( $\mu\text{mol/kg}$ )	TA ( $\mu\text{mol/kg}$ )	pH	$\Omega_{Ar}$	DIC ( $\mu\text{mol/kg}$ )	TA ( $\mu\text{mol/kg}$ )	pH	$\Omega_{Ar}$	DIC ( $\mu\text{mol/kg}$ )
0	2285,4	7,9825	1,790	2139,8	2517,7	7,4945	0,700	2542,4	2435,2	7,6874	1,031	2398,9	3099,3	7,0723	0,335	3461,5
2					2558,4	7,6464	0,992	2565,6					3487,0	7,3476	0,702	4144,7
4	2188,2	7,9512	1,607	2027,8	2559,9	7,6691	1,042	2487,7	2174,6	8,0265	1,857	2017,7	3666,3	7,3419	0,729	4184,3
6					2499,8	7,7469	1,202						3555,1	7,3956	0,796	4042,2
8	2118,0	7,9978	1,707	1932,1	2482,1	7,7722	1,259						3727,9	7,3790	0,805	4108,5
10					2446,0	7,7722	1,241	2338,2	1883,8	7,9833	1,470	1574,8	3578,2	7,3799	0,774	3810,8
14	2009,0	8,0395	1,756	1775,0	2359,3	7,8386	1,376	2148,2					3598,7	7,3476	0,724	3451,2
18					2342,5	7,8264	1,331		1756,2	7,8850	1,120		3596,5	7,3799	0,778	
20	1934,4	8,0668	1,782													

**Table A.6b** Measured and calculated carbonate system parameters of the blanks of the control experiment treatments. Values shown for  $\Omega_{Ar}$  were calculated by use of means of measured TA and pH (free scale) for a salinity of 33.3 and 15°C applying CO2SYS Excel Macro.

time (d)	non-bubbled						bubbled					
	Control (380 ppm CO <sub>2</sub> )			2400 ppm CO <sub>2</sub>			Control (400 ppm CO <sub>2</sub> )			2400 ppm CO <sub>2</sub>		
	TA (μmol/kg)	pH	$\Omega_{Ar}$	TA (μmol/kg)	pH	$\Omega_{Ar}$	TA (μmol/kg)	pH	$\Omega_{Ar}$	TA (μmol/kg)	pH	$\Omega_{Ar}$
0	2298,096	7,9921	1,835	2317,792	7,0949	0,264	2436,22	7,8470	1,447	2303,295	7,0438	0,234
2										2414,066	7,1178	0,289
6	2297,421	7,9741	1,769	2311,295	7,1518	0,299	2550,678	8,0901	2,480	2229,389	7,1267	0,273
12	2305,234	8,0123	1,917	2318,984	7,2421	0,368	2515,986	8,0972	2,479	2299,602	7,1077	0,269
18	2306,076	8,0171	1,936	2324,037	7,3547	0,474	2509,548	8,0352	2,189	2168,912	7,1035	0,252



Appendix 7 Statistical report for the control experiment

**Table A.7a** Non-linear regression applied for the 2400 ppm CO<sub>2</sub> treatment using dynamic fitting. Sigmoidal regression function after Chapman, 2 parameters.

Method	R <sup>2</sup>	Std. error of estimate	P	Power with $\alpha = 0.05$	DF	SS
non-bubbled	0.9696	0.0458	0.002	0.9997	7	0.3449
bubbled	0.9697	0.0317	0.002	0.9998	7	0.1658

P = probability, DF = degrees of freedom, SS = sum of squares

**Table A.7b** Non-linear regression applied for the 2400 ppm CO<sub>2</sub> treatment using dynamic fitting. Regression function for standard Michaelis-Menten kinetics, ligand binding, one site saturation.

Method	R <sup>2</sup>	B <sub>max</sub>	Std. deviation of B <sub>max</sub>	95 % confidence interval	DF	SS
non-bubbled	0.7742	1.2572	0.0501	1.135 to 1.38	6	0.0779
bubbled	0.9638	0.7948	0.0417	0.7589 to 0.8306	6	0.0060

DF = degrees of freedom, SS = sum of squares, B<sub>max</sub> = maximum reaction rate but corresponds here to  $\Omega_{Ar}$

Appendix 8 Unpaired t-test applied for ash-free dry weight of coral skeleton

**Table A.8** Unpaired t-test employed to test the colour varieties of *L. pertusa* for significant differences in the ash-free dry weight.

Colour variety	N	Mean	Std. deviation	Missing	SEM	P	Power with $\alpha = 0.05$	95 % confidence interval	DF
white	7	12.616	0.962	0	0.364	0.001	0.973	-4.079 to -1.299	11
red	6	15.305	1.313	0	0.536				

N = number of samples, SEM = standard error of mean, P = probability, DF = degrees of freedom

## Declaration of Academic Integrity / Selbstständigkeitserklärung

With this statement I declare that I have independently completed the above thesis, except for scientific consulting by my supervisors Dipl.-Biol. Armin Form/ Prof. Dr. Ulf Riebesell. The thoughts taken directly or indirectly from external sources are properly acknowledged. This thesis was not previously submitted to another academic institution.

Hiermit versichere ich, dass ich die vorliegende Arbeit selbständig verfasst und keine anderen als die angegebenen Quellen (siehe § 25, Abs. 7 der Diplomprüfungsordnung Biologie 2000) und Hilfsmittel verwendet habe.

Mir ist bekannt, dass gemäß § 8, Abs. 3 der Diplomprüfungsordnung Biologie 2000 die Prüfung wegen einer Pflichtwidrigkeit (Täuschung u.ä.) für nicht bestanden erklärt werden kann.

Rostock, den 27.10.2010

Janett Voigt